Journal of Quantitative Spectroscopy & Radiative Transfer 330 (2025) 109225

Contents lists available at ScienceDirect

Journal of Quantitative Spectroscopy and Radiative Transfer

journal homepage: www.elsevier.com/locate/jqsrt

Calculation of collisional line-broadening and shifting of acetylene using Complex Robert–Bonamy–Ma approach

Andrei Sokolov [a,*], Sergei N. Yurchenko [a,*], Jonathan Tennyson [a], Robert R. Gamache [b], Bastien Vispoel [c]

[a] Department of Physics and Astronomy, University College London, WC1E 6BT, London, UK
[b] Department of Environmental, Earth, and Atmospheric Sciences, University of Massachusetts Lowell, Lowell, MA, 01854, USA
[c] Research Unit Lasers and Spectroscopies, Institute of Life, Earth and Environment, University of Namur, Namur, B-5000, Belgium

ARTICLE INFO

Keywords:
Spectral line shapes
Semi-classical calculations
Acetylene

ABSTRACT

A comprehensive semi-classical study of the collisional line broadening and shift coefficients of C_2H_2 by several key perturbers (H_2, He, N_2, C_2H_2, CO, and CO_2) for astronomical applications using the Complex Robert–Bonamy–Ma (CRBM) framework is presented. Following the CRBM computational protocol, the intermolecular interaction potentials are constructed from atom–atom and electrostatic interactions, and then fitted to reproduce experimental room-temperature line-broadening parameters taken from the literature. In total, 657 experimental values are used in the fitting. The empirical potentials are then used to predict line broadening coefficients over a wide temperature range. Reference collisional line widths γ_0 and temperature exponents n for the commonly used single-power law are produced, as well as a set of parameters for the double-power law, which better reproduces the temperature dependence of theoretical predictions. The vibrational dependence of the line widths is studied using a new *ab initio* isotropic polarizability surface of C_2H_2 and is found to be negligible. The computed line broadening parameters are found to agree well with the experimental data, while the modelling of line shifts of HCCH is not satisfactory when compared to the experiment. The new line broadening data of C_2H_2 with the J (or m) dependence have been used to populate the ExoMol database www.exomol.com as part of the ExoMol pressure-broadening diet and can be used to model opacities of atmosphere of (extrasolar) planets. The CRBM methodology tested here on C_2H_2 can be used for other similar (closed-shell) systems in ExoMol that are important for exoplanetary atmospheric studies.

1. Introduction

Acetylene is a small polyatomic hydrocarbon species whose spectra are important in astrophysics and atmospheric studies [1]. On Earth, it is among the minor constituents of the atmosphere produced mainly by human activity [2]. It is also one of the target molecules being searched for on Mars in the 3 μm region [3,4]. Acetylene has also been detected in a number of other cooler bodies in the Solar system, such as Jupiter, Saturn, Titan, and Pluto, where the low-lying ν_5 fundamental band was observed. Outside the Solar system, various bands of acetylene have been observed in warmer environments such as carbon stars [5], hot Jupiters [6], and this molecule is predicted to be present in soot-rich sub-Neptune type extrasolar planets (exoplanets) [7]. In the context of atmospheres of exoplanets, acetylene is particularly intriguing because it can serve as a precursor for more complex organic compounds and, at high temperatures and high UV fluxes, may indicate a rich atmospheric chemistry.

The majority of known exoplanets are not visible directly, and disentangling their spectrum from that of a much brighter host star presents challenges. One of the main tools for detection of atomic and molecular species is cross-correlation, where the filtered high-resolution and noisy spectra of an exoplanet are compared against model planetary opacities for various species [8]. The need for accurate line positions and intensities has been recognized for some time now [9], and work is ongoing on generation of high-resolution molecular linelists within the frameworks of projects like HITEMP and ExoMol. Additionally, generation of cross-sections and opacities requires knowledge of the line shapes, which means that need for line broadening data is gaining increasing attention [10,11]. To address this challenge, theoretical studies of acetylene's spectral properties are crucial.

* Corresponding authors.
E-mail addresses: andrei.sokolov@ucl.ac.uk (A. Sokolov), s.yurchenko@ucl.ac.uk (S.N. Yurchenko).

https://doi.org/10.1016/j.jqsrt.2024.109225
Received 15 August 2024; Received in revised form 14 October 2024; Accepted 14 October 2024
Available online 2 November 2024

Broadening and shifting of acetylene lines by various perturbers has been extensively studied both experimentally and theoretically. Room-temperature measurements of multiple vibrational bands in pure acetylene have been performed by Jacquemart et al. [12,13]. Measurements in the ν_5, $\nu_4+\nu_5$, $\nu_1+\nu_3$, and $\nu_1+3\nu_3$ bands have also been performed by other groups [14–23]. Foreign-gas broadening and shifting has been studied in mixtures of acetylene with hydrogen [24–29], nitrogen [17,21,24,26–28,30–38], oxygen [33,35,39], rare gases [17,21,26–28,34,40], and carbon dioxide [35,41,42]. Theoretical studies were made using the close coupling approach [29,43], semi-classical Robert–Bonamy type calculations [44–47], and the fully classical Gordon's approach [48–50].

In this theoretical study, we use the semi-classical Complex Robert–Bonamy–Ma (CRBM) framework [51,52] and focus on the magnitude and temperature-dependence of acetylene broadening coefficients with various molecules relevant to astronomical applications over a wide temperature range. We also investigate the effect of vibrational contributions to line-broadening and lineshift coefficients. As for the collisional partners, in stars and in such exoplanets as hot Jupiters and sub-Neptunes, the primary broadening species will be molecular hydrogen H_2 and helium. We also include larger molecules that are likely to be present in the atmospheres of cooler and heavier atmospheres, such as CO_2, C_2H_2, CO, and N_2. The results are compared to existing experimental data and other theoretical approaches.

To assess vibrational contributions to line shape parameters, semi-classical approaches require knowledge of the state-dependent polarizabilities for acetylene. There are a number of theoretical and experimental studies on the polarizability of acetylene (see summaries in [53,54]), but few of them consider how this property changes with vibrational and rotational state. Russell and Spackman [55] calculated the electronic and rovibrational polarizabilities of acetylene using Møller-Plesset theory (MP2) and a more accurate Brueckner theory [56], BD(T). Monten et al. [57] investigated the dependence of polarizability of C_2H_2 on the number of perturbations included in coupled cluster expansion, as well as on completeness of the basis set. Sharipov et al. [58] aimed to cover dipole moments and polarizabilities for a vast number of small molecules, as well as to estimate vibrational contributions to these properties using DFT. We calculate the expectation values of the isotropic polarizability using a high-level CCSD(T)-F12b approach with the aug-cc-pVQZ basis set and variationally obtained ro-vibrational wavefunctions calculated using the variational program TROVE [59].

Our paper is organized as follows: Section 2 describes our methodology, including line shape calculation details, construction of the interaction potentials and their fitting, as well as details and results of the polarizability calculations. In Section 3, we show the results of line shape modelling and compare it with existing data; Section 4 provides a discussion of the results, and our Conclusions are given in Section 5.

2. Methodology

2.1. Collisional effects on shapes of isolated lines

Here we employ the Complex Robert–Bonamy–Ma framework [51,52] to study line-broadening and shifting coefficients of acetylene. In this semi-classical approach, the isolated-line halfwidths and shifts appear as averages of scattering matrix **S** over collision trajectories and perturber states [51],

$$(\gamma + i\delta)_{fi} = \frac{n_b}{2\pi c}\int_0^\infty v f(v) dv \int_0^\infty 2\pi\, b db \left(1 - \left\langle \mathbf{S}_{fi}\right\rangle_{J_2}\right), \tag{1}$$

where $\mathbf{S}_{fi} = \langle\langle v_i J_i v_f J_f|\hat{S}|v_i J_i v_f J_f\rangle\rangle$ is a matrix element of the scattering operator in line-space formed by Liouville-space vectors $|v_i J_i v_f J_f\rangle\rangle \equiv |v_f J_f\rangle\langle v_i J_i|$. The average over the perturber states was discussed by Ma et al. [52]. Because the subject of concern are isolated-line properties, the influence of line-mixing resulting from non-diagonality of the tetradic matrix **S** in line-space [60] is ignored here, and only two indices related to a spectral line $f \leftarrow i$ are retained. The elements of the scattering matrix depend on the details of intermolecular interactions which happen during the collisional event. To proceed with calculations, the scattering operator is expanded up to the second order in perturbation [61], and with the use of the cumulant expansion [62], the expression in the parentheses can be rewritten as

$$1 - \exp\left(-i\langle S_1\rangle_{J_2} - \langle S_2\rangle_{J_2}\right)_{f\leftarrow i}. \tag{2}$$

In this work, we also neglect the effects of line-coupling [63], which appear as a result of the non-diagonality of operators in this exponential. The S_1 term in the expression above is largely responsible for line shifting and the vibrational contribution to line-broadening and depends on the difference of angle-averaged interaction potentials in the initial and final states of the radiator $\Psi_{i,f}$ and the perturber Ψ_2:

$$S_1 = \frac{1}{\hbar}\int_{-\infty}^{\infty} dt\, \left[\left\langle \Psi_f\Psi_2\left|V^{\rm iso}(R(t))\right|\Psi_f\Psi_2\right\rangle - \left\langle \Psi_i\Psi_2\left|V^{\rm iso}(R(t))\right|\Psi_i\Psi_2\right\rangle\right]. \tag{3}$$

The dependence of the isotropic potential on v_2, J_2 will be ignored. The S_2 term is primarily responsible for the rotational dependence of line shape parameters within a vibrational band and is given by a sum of contributions $S_2 = S^*_{2,i2} + S_{2,f2} + S_{2,\rm middle}$, where the first two, "outer" terms are [64,65]

$$S_{2,i2} = \frac{1}{\hbar^2}\sum_{\substack{J_i' J_2' \\ l_1 l_2 \\ \mathbf{n_a}\mathbf{n_b}}} K_{\rm outer}\, D(l_1 l_2, \mathbf{n_a}\mathbf{n_b}, J_i J_i' J_2 J_2')\, F^{l_1 l_2}_{\mathbf{n_a}\mathbf{n_b}}(\omega_{J_i J_i'} + \omega_{J_2 J_2'}), \tag{4}$$

and the $S_{2,f2}$-term is obtained by index interchange $i \leftrightarrow f$. The "middle" term is [63,64]

$$S_{2,\rm middle} = \frac{1}{\hbar^2}\sum_{J_2'}\sum_{\substack{l_1 l_2 \\ \mathbf{n_a}\mathbf{n_b}}} K_{\rm middle}\, D\left(l_1 l_2, \mathbf{n_a}\mathbf{n_b}, J_i J_f, J_2 J_2'\right)\, F^{l_1 l_2}_{\mathbf{n_a}\mathbf{n_b}}\left(\omega_{J_2 J_2'}\right). \tag{5}$$

In the above equations, D is a product of reduced matrix elements of the kind $\langle\Psi_i\|D^l_{*n}(\Omega)\|\Psi_{i'}\rangle$. For various collisions, their contribution is usually diminished by resonance functions F which contain the time-integral of the interaction and help satisfy the energy balance in the scattering matrix [66]. K is a numerical factor coming from recoupling coefficients, $\mathbf{n_k} = n_{k,i}$ with $k = a, b$, $i = 1, 2$ is a pair of indices for each molecule coming from the two terms in this second-order perturbational treatment, which along with $l_{1,2}$ appear in the interaction potential expansion.

The time dependence in both S_1 and S_2 is contained in the integral of $V(R(t))$, that is the strength of interaction between the two molecules during collisions, which are assumed to follow classical trajectories given an initial relative velocity v and impact parameter b. $R(t)$ is the centre-of-mass separation of the two colliding molecules at time t. Instead of assuming a trajectory model (straight-line or parabolic), the trajectories are numerically integrated using Hamilton's equations and the isotropic part $V^{\rm iso}(R(t))$ of the interaction potential ("exact" trajectories). This ground-vibrational-state isotropic potential was used for trajectory calculations for all the vibrational states of the radiating molecule. Once the classical paths are established, we calculate the components of the scattering matrix S_1 and S_2. The S_1 term only depends on the isotropic part of the potential, and its vibrational dependence is included through modification of long-range van-der-Waals interactions. The S_2 term, on the other hand, only depends on the anisotropic terms, and those are constructed using a vibration-independent potential with electrostatic and atom–atom contributions.

2.2. Interaction potential

Theoretical determination of line shape parameters relies on the details of interaction between the radiator and perturber during the collisional event. The scattering matrix elements from Eq. (1) need to be calculated for a number of initial velocities, impact parameters and internal states of the molecules. An account of the full interaction potential and the resulting exact (no quotes) trajectories are not easy to include in a semi-classical approach. One consequence is the emerging energy exchange between rotational and translational motions, which is usually ignored in semi-classical methods. Another one is out-of-plane trajectories which are no longer symmetric with respect to the distance of the closest approach $r_c = r(t = 0)$ and would require a general expression for the resonance functions, without any analytical simplifications. In the current approach, the trajectories resulting from different initial conditions are assumed to be propagated by the isotropic potential, and at each moment the value of the full interaction potential is used for the calculation of S_1 and S_2 terms.

To this end, we construct model potentials, V, for C_2H_2+X (X=H_2, He, N_2, C_2H_2, CO_2, CO) as follows. The molecules are considered to be rigid rotors with equilibrium geometries taken from the ground electronic state. This choice helps us reduce the dimensionality of the problem to the monomer rotation degrees of freedom only. The interaction potential is constructed from two parts as

$$V = V_{\text{estat}} + V_{\text{a-a}}. \tag{6}$$

Here, the long-ranged electrostatic interactions between molecules, V_{estat}, are described with the usual expressions for the interaction between electric multipoles [67] and expressed as a series in spherical harmonics. The second term $V_{\text{a-a}}$, predominantly responsible for the short-ranged interactions, is built from individual atom–atom contributions that use the Lennard-Jones (LJ) 6-12 form as given by

$$V_{\text{a-a}} = \sum_{i=1}^{n}\sum_{j=1}^{m} 4\varepsilon_{ij}\left[\left(\frac{\sigma_{ij}}{r_{1i,2j}}\right)^{12} - \left(\frac{\sigma_{ij}}{r_{1i,2j}}\right)^{6}\right]. \tag{7}$$

To cast this into the same form as used for electrostatic interactions, the two-centre expansion [67] is applied to $V_{\text{a-a}}$ using both molecules' equilibrium geometries and the relative orientation of the molecules in the dimer. With the atom–atom potential expressed as $V_{ij} = \sum a_n R^{-n}$ (see above), the general expression for the interaction potential in laboratory-fixed frame (LFF) can be written as

$$V(R,\Omega_1,\Omega_2,\omega) = \sum_{l_1 l_2 l}\sum_{\substack{n_1 n_2\\ m_1 m_2\\ m}}\sum_{w,q}\frac{U\left(l_1 l_2 l, n_1 n_2 wq\right)}{R^{q+l_1+l_2+2w}} \times C^{lm}_{l_1 m_1\, l_2 m_2} D^{l_1}_{m_1 n_1}{}^{*}\left(\Omega_1\right) D^{l_2}_{m_2 n_2}{}^{*}\left(\Omega_2\right) Y_{lm}{}^{*}(\omega). \tag{8}$$

Here, $C^{lm}_{l_1 m_1\, l_2 m_2}$ is the Clebsch–Gordan coefficient, $D^{l}_{mn}(\Omega)$ are Wigner D-matrices, and $Y_{lm}(\omega)$ are spherical harmonics. Together, these terms form the rotationally invariant part of the potential which depends on the orientations of molecular axes $\Omega = (\alpha, \beta, \gamma)$ in LFF and the direction $\omega = (\theta, \varphi)$ of a vector $\vec{R}$ connecting the centres of masses of the two molecules. $U(\dots)$ is the expansion coefficient representing the combined contribution from electrostatic and atom–atom interactions for a particular power in R. The summation is performed over various symmetries of the interaction l_1, l_2, different projections n, m entering the rotationally-invariant term, and integer indices w and q. The latter is equal to 1 for electrostatic terms and 6 or 12 for the atom–atom terms. All the molecules which we consider as rigid are linear at equilibrium, so the above expression somewhat simplifies with $n_1 = n_2 = 0$. As for the truncation of other expansions, in this work we used the 4th rank ($\max(l_1, l_2)$) and 20th order ($l_1 + l_2 + 2w$) to ensure convergence with respect to both angular and radial variables.

The isotropic potential used in trajectory propagation can be obtained from Eq. (8) by choosing the $l_1, l_2, l = 0$ contribution from the expansion. For some of the systems, as will be demonstrated below, a simplified m-n LJ version of the potential was used instead, expressed through parameters σ_{iso}, ε_{iso}:

$$V_{\text{iso}} = 4\varepsilon_{\text{iso}}\left[\left(\frac{\sigma_{\text{iso}}}{r}\right)^{m} - \left(\frac{\sigma_{\text{iso}}}{r}\right)^{n}\right]. \tag{9}$$

2.3. Effects of vibrational dephasing

In the current approach, vibrational contribution to the line-shape parameters can be reduced to several effects [68,69] that affect the values of S_1 and S_2. The first one affects both contributions and comes from a difference in classical trajectories. When the target molecule is vibrationally excited it has a different effective equilibrium geometry meaning that the classical trajectories describing the collision will also be slightly different. We neglect this effect as it is expected to only matter for very weakly interacting partners [69], so a single time-integration is done in Eq. (3) for each pair of states i, f.

The other effects appear as differences in individual S_1 and S_2 contributions compared to purely rotational transitions. The changes in the S_2 term, come from small changes in the energy gaps, the rotational parts of wavefunctions and the collisional transition probabilities for different rovibrational states. The energy gaps $\Delta E_{i,i'} - \Delta E_{J_2,J_2'}$ were calculated using energies of acetylene and the perturbers taken from the ExoMol database [70]. The wavefunctions and respective transition probabilities, related to reduced matrix elements $\langle \Psi_i \| D^{l}_{*n}(\Omega) \| \Psi_{i'} \rangle$, can be calculated using *ab initio* wavefunctions [71]. However, in this work we employ a simplified approach which used rigid linear rotor wavefunctions $|JKM\rangle = |J0M\rangle$ for the S_2 term. Also, the matrix elements are calculated only for collisional transitions within a given vibrational state, so collisional transitions between states belonging to different vibrational states are not considered here due to the isolated vibrational state assumption; because of this approximation, the averaging in Eq. (1) is only performed over one (ground) vibrational state.

We now focus on the description of the S_1 term which includes most of the vibrational contribution to the line shape. From Eq. (3) it follows that S_1 is non-zero only if the isotropic part of the potential shows dependence on the radiating-molecule state. To account for the dependence of the isotropic potential on the radiator state, we follow the usual practice and introduce a separate potential showing this rovibrational dependence which is approximated using only van der Waals dispersion interactions as $-C_6/R^6$. The respective expectation values for a particular state g that would enter Eq. (3) can be written as

$$\langle \Psi_{a,g} | V^{\text{iso}}(t) | \Psi_{a,g} \rangle = -\frac{3\alpha_b \bar{U}}{2R^6(t)} \langle \Psi_{a,g} | \alpha_a | \Psi_{a,g} \rangle, \tag{10}$$

where α is the isotropic polarizability tensor, a and b designate the radiating molecule and the perturber, $g = i, f$ is the initial (final) states of the radiating molecule, $\bar{U}$ is the mean excitation energy, and the expectation values are taken over the radiating-molecule states. We emphasize that this representation of the potential is only used for the calculation of the (ro)vibrational-state dependence of the S_1 term, while both the molecular trajectories and the S_2 contributions are calculated using the potential expressions described in the previous section.

We explored two expressions to calculate the dispersion interaction energy. One is the London formula,

$$C_6^{\text{Lond}} = \frac{3}{2}\bar{U}\alpha_a^{\text{iso}}\alpha_b^{\text{iso}} \quad [\text{eV}\cdot a_0^6], \tag{11}$$

where the mean excitation energy $\bar{U}$ is related to the ionization potentials via the Unsöld approximation [72]

$$\bar{U} = I_a I_b/(I_a + I_b)$$

with I in eV and α in a_0^3. This is the most popular method in the literature to estimate changes in the long-range interactions. An alternative approach is to use the Slater–Kirkwood formula, which employs a different expression for $\bar{U}$ and reads

$$C_6^{\text{Sl-Kirk}} = \frac{3}{2}\frac{a_0^{3/2}}{\left(\alpha_a^{\text{iso}}/N_a\right)^{1/2} + \left(\alpha_b^{\text{iso}}/N_b\right)^{1/2}}\alpha_a^{\text{iso}}\alpha_b^{\text{iso}} \quad [\text{Ha}\cdot a_0^6]. \tag{12}$$

Calculations using Eqs. (11) and (12) require knowledge of the expectation values of the polarizability, calculations of which will be discussed in detail below. Additionally, one needs ionization potentials I or effective number of electrons N depending on which formula is chosen. In our calculations, values α_b^{iso} and $I_{a,b}$ were taken from the NIST database [73] and $N_{a,b}$ were taken from expressions given in [74]. The state-dependent polarizability values of the radiator have been computed by us as will be described in the next section.

We also explored two modifications of the potential in Eq. (10) for the S_1 term. One is to include an approximate effect of the vibrational motion on the short-ranged forces such as C_{12}/r^{12} using expressions from [74] with the C_{12} coefficient estimated from molecular polarizabilities. Although the change in the repulsive part with rovibrational state is usually neglected, it might be more relevant for systems with weaker electrostatic interactions like for acetylene which has no permanent dipole moment.

The second modification consists of a different way to set up $V^{\text{iso}}(R;vJ)$ in Eq. (3). Instead of introducing a separate isotropic potential for use just with S_1, we scaled the LJ coefficients of the existing ground-vibrational-state potential used for trajectory propagation. The LJ parameters of that potential expressed by Eq. (10) are scaled by $\sigma_{v\neq0}/\sigma_{v=0}$ and $\varepsilon_{v\neq0}/\varepsilon_{v=0}$, where the scaling coefficients are based on calculated values of polarizabilities and London or Slater–Kirkwood expressions. This option can help avoid a situation where the two potentials estimated from different grounds (atom–atom + electrostatic, Eq. (9) vs polarizability based, Eq. (10)) have noticeably different values of σ_{iso}, so that collisions never get molecules close enough to where the short-range part of the second potential would come into play.

As will be demonstrated below, our calculated acetylene linewidths are not very sensitive to these ways of computing S_1. The effect is small and indistinguishable within experimental uncertainties, while accuracy of lineshift predictions for any of these approaches listed above falls short of expectations.

2.4. Interaction potential fitting

Usually, the broadening parameters calculated with semi-classical (*ab initio*) approaches are slightly overestimated (see, e.g., Refs. [64,75–79]) and predictions with such models can be substantially improved by fitting the interaction potential to minimize the difference between theoretical and experimental broadening parameters, which can be done through a non-linear least squares fit. Below, we describe which parameters were fitted, what were they fitted to and how the residuals were constructed.

In the atom–atom part of the potential in Eq. (7), the major source of uncertainties lies in the LJ parameters σ_{ij} and ε_{ij} in Eq. (7) between different atoms of acetylene and those of the perturber (C–H, C–He, H–H, etc.). These quantities are not always well known or necessarily transferable between different molecules, so they are fitted for each pair of atoms for each collisional system. For example, the C_2H_2–H_2 system requires two types of interactions, C–H and H–H, while for C_2H_2–CO_2 dimer there are four different pairs of interactions, each of which has two parameters, σ_{ij} and ε_{ij}. In this work, the initial estimates for atom–atom parameters of C_2H_2–X were either taken from the literature [80,81] or from our previous works (i.e., [82,83]). Where necessary, the interaction parameters were constructed from homonuclear tabulated Lennard-Jones values using Lorentz–Berthelot combination rules [81].

Table 1
Sources for line broadening/shifting data at room temperature used in this study.

Source	Perturber	Band	Line profile
[25]	H_2	ν_5	V
[32]	N_2	ν_5	V
[14]	C_2H_2	ν_5	V
[27]	H_2, He	ν_5	–
[28]	H_2, He, N_2	$\nu_1+\nu_3$	V
[26]	H_2, He, N_2	ν_5	V
[31]	N_2	$(\nu_4+\nu_5)^0$	V
[17]	He, N_2, C_2H_2	$\nu_1+3\nu_3$	G, R
[40]	He	ν_5	V
[16]	C_2H_2	$\nu_1+3\nu_3$	V
[18]	C_2H_2	$(\nu_4+\nu_5)^0$	V
[12]	C_2H_2	three bands	R
[36]	N_2	$(\nu_4+\nu_5)^0$	R
[37]	N_2	$(\nu_4+\nu_5)^0$	V
[41]	CO_2	$(\nu_4+\nu_5)^0$	R
[42]	CO_2	ν_3	V
[35]	CO_2	$\nu_1+\nu_3$	V

Line profiles are denoted by R: Rautian, G: Galatry, V: Voigt, or "–": not specified.

As for the electrostatic part, it has been established that Robert–Bonamy (RB) type calculations for acetylene show better agreement with the experiment when using a smaller quadrupole moment value than predicted by experiment or theory (i.e., [18,45,84]). Given how the electrostatic interactions involving its quadrupole are dominant for acetylene line broadening values, we chose to treat the quadrupole moment of acetylene as an adjustable parameter, which is fitted for each broadener case. The quadrupole moments θ (and additionally the dipole moment μ for CO), required for the calculation of electrostatic interactions and equilibrium geometries of individual perturbing molecules were taken from NIST [73].

The third set of parameters, in addition to LJ parameters $\{\sigma_{ij},\varepsilon_{ij}\}$ and the quadrupole moment θ, are the isotropic potential parameters σ_{iso} and ε_{iso} used to propagate the trajectories. Generally, this isotropic potential is drawn from the expansion in Eq. (8) by setting $l_1,l_2,l=0$. However, this can only be done reliably if the potential is known to be accurate. Because the parameters $\{\sigma_{ij},\varepsilon_{ij}\}$ and q already act as effective ones, in some cases we instead fit σ_{iso} and ε_{iso} from Eq. (9) or fix them to known *ab initio* values instead of using the expansion. The quality of the fit is quantified with the root mean squared error defined as

$$\text{rmse} = \sqrt{\frac{1}{N-P}\sum_{i=1}^{N}\left(\gamma_i^{\text{expt}} - \gamma_i^{\text{theory}}\right)^2},$$

where N is the number of experimental points and P is the number of interaction potential parameters varied in a particular fit.

2.5. Choice of experimental line shape data

The reference pressure broadening coefficients data used in fitting of the potentials were taken from the available experimental sources for P- and R-branches at room temperature and are listed in Table 1. Although this set is not exhaustive and more experimental data can be found in Refs. [12,45] and some newer papers, including different temperatures, bands, perturbers, and model profiles, we use it as a representative sample of broadening and shifting data for at least a couple of different bands for each of the five perturbing species considered with available experimental data with the aim of investigating the presence of vibrational dependence. Some experimental data were not considered if we already had reliable data with good coverage of lines for that particular band, or if the data were found to have systematic errors comparing to more reliable data from other publications. Lower-temperature data were not considered because we target higher temperature applications and, additionally, the fitting procedure could perform worse due to poor predictions of semi-classical methods

at lower temperatures. The scarce high-temperature data, where semi-classical methods should perform well, were reserved as a test group for our theoretical predictions.

Ideally, one would require accurate measurements of widths and shifts both at small and large values of J for different vibrational states and covering a large temperature range. Provided the theory is sound and the experiment is sufficiently accurate, even a few measurements constraining both the long- and the short-range parameters of the interaction potential should suffice to obtain accurate theoretical temperature-dependent line shape parameters [85]. However, these demands are often not met due to time constraints or experimental obstacles such as temperature/pressure limitations, safety concerns (as in the case of the hot acetylene), high noise in low-intensity lines, high uncertainties in shifts measurements, as well as data treatment difficulties in signal analysis [13,35,41,86].

Another issue comes from the use of different line profiles in experimental retrievals. CRBM is suited to describe the Lorentzian part of the observed line profile and can provide [87] the parameters γ_0, δ_0, γ_2, and δ_2 of the quadratic speed-dependent Voigt profile (qSDVP). Velocity-changing collisions are not a part of this model. Thus, it would be appropriate to fit our results on experimental broadening parameters retrieved with the same qSDVP model. If we look at the broadening parameters in Table 1, most of them were obtained from the Voigt-profile fits. However, there is little discussion about possible deviations from the Voigt shape. Recent discussion [22,23,88,89] has revealed that using the Voigt profile in retrievals can lead to unphysical halfwidth alternations between even and odd Js, while the use of qSDVP gives a much more accurate description. Some publications use the Rautian or Galatry profiles instead of qSDVP to reduce their measurements, which also leads to better residuals. However, those profiles include the effects of velocity-changing collisions that are absent in our model. Sometimes retrievals are presented for multiple profiles (see, e.g., Ref. [37]) where the differences in γ_0 reach ~ 0.004 cm^{-1}atm^{-1} ($\sim 5\%$). At the same time, the experimental data (see Table 1) that use different profile models lie roughly within each other's error bounds. For this reason, we decided to ignore any differences between the underlying models used in retrievals and treat all experimental and theoretical γ_0 values as comparable, regardless of the profile. All the data were weighted by the corresponding experimental uncertainty in our fitting procedure.

2.6. Fitting procedure details

The fitting of interaction potential parameters σ_{ij}, ϵ_{ij}, θ, (σ_{iso}, ϵ_{iso}) was performed in python with a non-linear least squares minimization package using trust region reflective algorithm [90]. The individual dimensionless residuals for each point were constructed as

$$r_i = \frac{A_i^{\text{theory}} - A_i^{\text{expt}}}{\sigma_i^{\text{expt}}} \tag{13}$$

to minimize the effect of experimental data with large error bars. Here, A_i^{theory} are the calculated values of γ (δ) at each iteration, and A_i^{expt} and σ_i^{theory} are experimental values and their uncertainties. The Jacobian used to determine the steepest descent path was computed numerically by finite differences (5% deviations from value at current iteration) in each of the fitting parameters.

We performed calculations for each of the bands and compared them only to data from that particular band instead of polling together all the data for each J as v-independent. This makes the procedure less robust if data for one particular band are erroneous but allows for testing of the vibrational dependence in the calculation. This procedure also allows for the inclusion shifts in the residual, but we later found that it also makes the convergence worse, so fitting was only done using the broadening data. The residuals vector to be minimized is then

$$\vec{r} = \left\{ r_{1,1}^{\text{HW}}, r_{1,2}^{\text{HW}}, \ldots, r_{k,n}^{\text{HW}} \right\}, \tag{14}$$

where k is the counting number of a band and n is the number of experimentally measured lines in that band.

The performance of non-linear least squares algorithms strongly depends on the details of the algorithm, so multiple fits for each collisional system have been performed using different initial potential parameters from the literature, different ways of numerical Jacobian evaluation, in-built loss functions, and fixing some parameters during fitting. Sometimes, the fits converged to some local minima and the broadening coefficients with those input parameters were not satisfactory. In some other cases, visually indistinguishable broadening predictions were obtained using different values of interaction potential parameters because of the in-built uncertainty in non-linear fits coming from parameter-space curvature. The final potential parameters were chosen from among the fits such that the broadening coefficients were closest to the experiment and showed no unphysical behaviour at high J where there is no experiment to constrain the fits.

2.7. Rovibrationally averaged polarizabilities

Often when S_1 is included in line shape calculations, only the vibrational matrix elements are used in Eq. (10). Such an approach is exact if rovibrational interactions for states in a certain energy range are small in magnitude, in which case the matrix elements are independent of J [91]. However, in the general case some influence of the rotational state on the interaction potential can be expected. Here we use accurate rovibrational wavefunctions of C_2H_2 generated variationally using the rovibrational program TROVE [59] to compute the matrix elements of $V_{\text{disp}}^{\text{iso}}$ in conjunction with a high level *ab initio* polarizability surface α. Using accurate nuclear motion wavefunctions helps account for the contributions from both vibrational and rotational degrees of freedom of the radiator to the intermolecular potential. It has been argued, that for the line shifts in the water's ν_2 and $\nu_2 + \nu_3$ bands, this effect is important [92]. As will be shown below, accounting for these effects for acetylene does not affect the broadening and shifts significantly.

The calculations of the rovibrationally averaged isotropic electric polarizabilities follow the Born–Oppenheimer approach and is performed in two steps. In the first step, the electronically averaged polarizability surfaces of C_2H_2 are computed with the MOLPRO 2020 program [93]. We used the CCSD(T)-F12b/AVQZ level of theory [94] to compute the matrix elements of the static polarizability tensor for an isolated electronic state as

$$\alpha_{ij}(\mathbf{r}) = \left. \frac{\partial^2 E(\mathbf{r}; F)}{\partial F_i \partial F_j} \right|_{F=0}, \tag{15}$$

on a large set of geometries (37400) covering the energy range up to 26,000 cm^{-1}. Here, $E(\mathbf{r}; F)$ are the energies, $i, j = x, y, z$ are directions of the field given in molecule-fixed frame, $\mathbf{r}$ represent the molecular geometry and F are the field strength. This derivative can be calculated numerically using the finite-field method with sufficiently small values of F_i (we used $F_i = 0.005$ a.u.) to exclude the effects of hyperpolarizabilities but large enough to ensure numerical accuracy. We then obtain the isotropic polarizability surface as

$$\bar{\alpha}(\mathbf{r}) = (\alpha_{xx}(\mathbf{r}) + \alpha_{yy}(\mathbf{r}) + \alpha_{zz}(\mathbf{r}))/3.$$

It is also implicitly assumed, that the pure vibrational contribution to polarizability are neglected as the response of nuclei to the field is too slow, so only the fast response of electrons is taken into account.

Some comparison of our results with the polarizability values of acetylene from the literature is presented in Table 2, where one can see that with a sufficiently large basis set and enough terms to describe electron correlation, the values $\bar{\alpha}_e$ are within several $\sim 0.1\ a_0{}^3$.

In the rovibrational calculations with the variational code TROVE we employ the same calculation setup as in Chubb et al. [95], where it has been used to compute an extensive line list aCeTy for acetylene. This includes an empirical PES obtained by fitting to the experimentally

Table 2
Values for the polarizability of acetylene in units $a_0{}^3$. Note that the zero-point corrections $\Delta\bar{\alpha}_{\mathrm{ZPC}}$ often designate different quantities; see text for details. Molecular geometries were often calculated with a different basis, which is not given here.

Method	$\bar{\alpha}_e$	$\Delta\bar{\alpha}_{\mathrm{ZPC}}$
CCSD(T)/AVQZ[a] [57]	22.504	0.50[b]
CCSDTQ(P)/CBS [57]	22.476	0.50[b]
MP2/TZP2(f) [55]	22.711	0.45[b]
BD(T)/TZP2(f,d) [55]	22.554	0.45[b]
B97-2/Sadlej pVTZ [58]	23.474	0.59[c]
MP4(SDQ)/Sadlej pVTZ [58]	22.643	0.59[c]
CCSD(T)-F12b/AVQZ[a] (this work)	22.625	0.73[b]

[a] AVXZ = aug-cc-pVXZ.
[b] Correction for ground vibrational state, $J = 0$.
[c] Average at 298 K.

derived energies of C_2H_2 from Chubb et al. [96]. The Hamiltonian operator, including the kinetic energy operator and potential energy function, was represented as a Taylor-type expansion in terms $3N-5 = 7$ linearized coordinates $\boldsymbol{\xi}$ $\{\xi_1, \xi_2, \ldots, \xi_7\}$ [97] given by

$$\begin{aligned}
\xi_1 &= (r^{\mathrm{lin}}_{\mathrm{CC}} - R_e), \\
\xi_2 &= (r^{\mathrm{lin}}_{\mathrm{CH}_1} - r_e), \\
\xi_3 &= (r^{\mathrm{lin}}_{\mathrm{CH}_2} - r_e), \\
\xi_4 &= \Delta x_1, \\
\xi_5 &= \Delta y_1, \\
\xi_6 &= \Delta x_2, \\
\xi_7 &= \Delta y_2.
\end{aligned} \tag{16}$$

Here, $r^{\mathrm{lin}}_{\mathrm{CC}}$, $r^{\mathrm{lin}}_{\mathrm{CH}_1}$ and $r^{\mathrm{lin}}_{\mathrm{CH}_2}$ are linearized (in terms of the Cartesian displacements) bond length values and Δx_1, Δy_1, Δx_2 Δy_2 are the Cartesian displacements of the hydrogen atoms in the $(3N-5)$ representation [97]. The D_{20h}(M) molecular symmetry group [98] was used for symmetry adaptations of the basis set functions with the TROVE automatic symmetrization procedure [99]. The primitive vibrational basis set was limited by the polyad number scheme:

$$P = 2n_1 + n_2 + n_3 + n_4 + n_5 + n_6 + n_7 \le 12,$$

where n_i are the excitation numbers of the 7 one-dimensional vibrational sets, with $i = 1$ corresponding to the C–C mode, while $i = 2, 3$ correspond to the two C–H stretches and $i = 4, 5, 6, 7$ correspond to the four Cartesian-like bending modes (see [97]).

The isotropic polarizability $\bar{\alpha}$ is then represented using a Taylor-type expansion in terms of the same 7 linearized coordinates ξ_n $(n = 1, \ldots, 7)$ as in Eq. (16):

$$\bar{\alpha}(\boldsymbol{\xi}) = \sum_{i,j,k,\ldots} F_{i,j,k,\ldots} \xi_1^i \xi_2^j \xi_3^k \ldots \tag{17}$$

where $F_{i,j,k,\ldots}$ are expansion parameters obtained through a least-squares fit the *ab initio* values of $\bar{\alpha}(\boldsymbol{\xi})$.

The TROVE rovibrational wavefunctions were computed and used to obtain rovibrationally averaged polarizability matrix for a number of vibrational states v and $J = 0 \ldots 30$ as expectation values

$$\bar{\alpha}_{v,J} = \langle v, J | \bar{\alpha}(\boldsymbol{\xi}) | v, J \rangle,$$

where v is a short hand notation for a vibrational state of acetylene $v_1, v_2, v_3, v_4^{l_4} v_5^{l_5}$.

The result represents electronic polarizability with a correction coming from a different effective geometry in a particular rovibrational state. Note, that this quantity is different from the purely vibrational contribution [100] (sometimes also confusingly called "atomic" or "geometric") caused by a change in vibrational wavefunctions under the influence of electric field, that is a change in nuclear and not electronic motion.

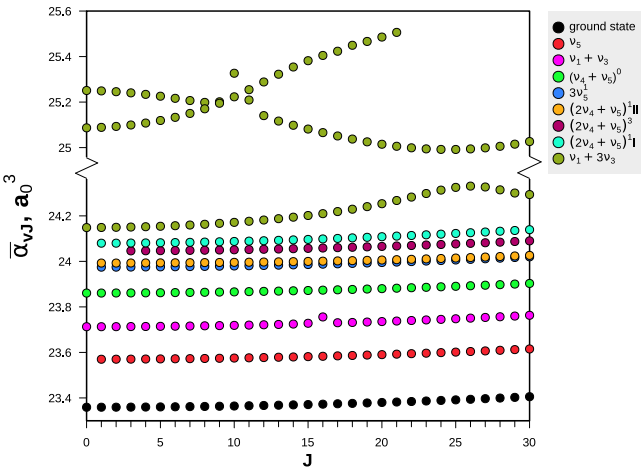

Fig. 1. Calculated expectation values of polarizability for selected states.

The data calculated for nine vibrational states considered in this work is shown in Fig. 1. A table with numerical values is given in the supplementary material. Each vibrational state shows a slight rotational (J) dependence which can be modelled as a quadratic function of J, at least outside any interactions or resonances. When the latter occur, the single state dependence changes to a more complex avoided-crossing-type pattern or gives rise to outliers. At lower energies this is fairly rare (only one point for the $\nu_1 + \nu_3$ state), but as energy and the associated density of states increase, the rotational dependence of the expectation values of polarizabilities becomes increasingly non-monotonic. As an example, the figure shows the complicated J-dependence of the $\nu_1 + 3\nu_3$ state (lowest dark green curve), as well as a complicated behaviour of two other states from the same polyad, as illustrated by the dark green curves in the top part of the figure.

Given the polarizability value of the ground vibrational state at $J = 0$, the zero-point correction is calculated as $\bar{\alpha}_{\mathrm{gs},J=0} - \bar{\alpha}_e = 0.73\ a_0{}^3$. From examining Table 2, one can see this value is higher than the others. The study [57] estimates their zero-point correction to electronic polarizability using the Born–Oppenheimer molecular dynamics, which leads to a correction at $T = 298$ K of $\Delta\alpha = 0.50\ a_0^3$. The difference with [57] cannot be attributed to the temperature effect, given that at room temperature about $\sim 85\%$ of molecules occupy the ground vibrational state and our data for $\bar{\alpha}_{v,J=0}$ is larger than their average, but to the potential energies and/or wavefunctions used. We do not know the exact cause but possible impacts on the broadening from this difference are discussed below.

3. Results of CRBM calculations

The model described above was used with the CRBM code to compute line broadening and line shift parameters for C_2H_2 perturbed by six species: H_2, He, N_2, CO, CO_2, and self-broadening. For each perturber, a number of non-linear least-squares fits to adjust the potential based on experimental broadening data (see Section 2.4) were performed. We only present a few of these fits in detail to illustrate the quality of predictions with and without fitting of the interaction potential parameters. The list of parameters producing the best fit for each of the perturbers is given in the Supplementary material. Calculations of broadening parameters showed only a small dependence on the vibrational band, so results are shown only for one band for all the perturbers except for nitrogen, where the vibrational dependence is examined in more detail.

3.1. Line broadening coefficients

3.1.1. C_2H_2–H_2

As mentioned above, semi-classical broadening coefficients are often overestimated, and for the case of broadening by light molecules this effect is more pronounced. In practical applications, the common solution is to refine the interaction potentials parameters as described above by fitting to the experimental values of the line broadening parameters γ. In fact, fitting is essential to ensure reasonable reproduction of the experiment and, more importantly, reliable predictions. In fits for C_2H_2–H_2, we used 104 experimental measurements of γ at room temperature with $|m|$ spanning from 1 to 37 taken from Refs. [25,26,28].

Fig. 2 shows line broadening parameters for C_2H_2 perturbed by hydrogen at room temperature, obtained using the three interaction potentials obtained from different combination rules and two fitted results for the $\nu_1 + \nu_3$ band. We observed no significant vibrational dependence of the broadening parameters, so only data for this band are presented. Our theoretical data are compared with the experimental values (ν_5 and $\nu_1 + \nu_3$ bands) and to the Robert–Bonamy calculations from Thibault et al. [76] which use an accurate *ab initio* potential [101]. Broadening coefficients are plotted against a spectroscopic parameter $|m|$ defined as

$$m = -J, \quad \text{(P-branch)}$$
$$m = J + 1, \quad \text{(R-branch)}$$
$$m = J. \quad \text{(Q-branch)}$$

Regardless of the choice of the interaction potential used, without refinement, the CRBM values of the C_2H_2–H_2 broadening parameters are significantly larger than experimental values. The same applies to the RB calculations by Thibault et al. [76] shown with green circles, although the difference is smaller.

We would like to stress that though this comparison looks unfavourable for CRBM, the original RB method had a minor mistake in the averaging expression that has since been fixed [52], so CRBM (and similar, newer methods like CRBM with line coupling, CRBMc [63]) should be preferable being more theoretically sound. Fitting of interaction potential parameters substantially ameliorates our agreement with the experiment. Fit 1 which starts from starting estimate 1 (red points) uses five parameters, two pairs of atom–atom parameters for C–H, H–H and θ taken from [44], and the isotropic 6-12 LJ potential is obtained from this potential's expansion. Fit 2 starts from starting estimate 2 (blue points) and uses seven fitting parameters, fitting the isotropic interactions as well. It uses the same atom–atom parameters and θ, and the isotropic potential is estimated from molecular polarizabilities and expressions in [74]. Fitting gives rmse of 0.0034 $cm^{-1}atm^{-1}$ and 0.0029 $cm^{-1}atm^{-1}$ at room temperature for fits 1 and 2, respectively. For reference, the J-averaged experimental errors are 0.0044 [25], 0.0014 [26], and 0.0038 $cm^{-1}atm^{-1}$ [28], respectively, but the experiments do not perfectly agree among each other, and figures better show the quality of the fit.

Fig. 3 shows the fitted results in more detail. The experimental values of γ of C_2H_2–H_2 exhibit a mild slope with increasing $|m|$ (or J), which is well reproduced in our calculations. The calculated values appear to be underestimated for the first couple of lines, while the rest of the values lie well within the experimental bounds. It is interesting, that the close coupling calculations from Thibault et al. [76] (orange circles) show additional depression in broadening coefficients around $|m| \approx 6$ which is not apparent in the experiment or our calculations. The trend at intermediate values of $|m|$ (or J) is consistent among all datasets. At higher Js, the large experimental uncertainties make it harder to constrain the results of our fits, which continue to show a mild decline. The HITRAN [102] data for this system, being empirical in nature, shows great agreement at small and intermediate $|m|$, but γ is simply set to a constant value for high J values. Still, this should

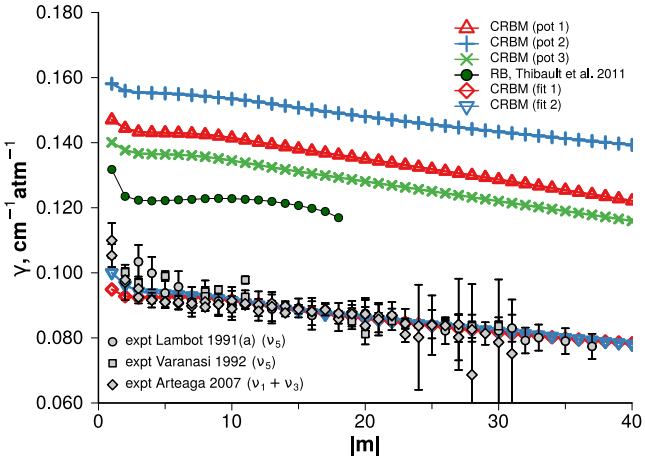

Fig. 2. Comparison of broadening coefficients for C_2H_2–H_2 at room temperature with and without fitting. Experimental data from [25,26,28], theoretical data for comparison from [76].

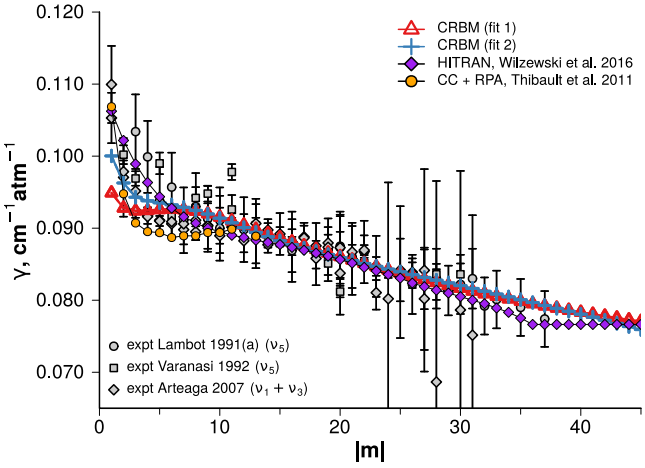

Fig. 3. C_2H_2–H_2 broadening coefficients at room temperature. Experimental data from [25,26,28], theoretical data for comparison from [76,102].

not be interpreted as a significant drawback because the intensities of lines with high J will likely be small even at high temperatures and the resulting discrepancy in the cross-sections will be minimal.

As there are no experimental broadening data for C_2H_2–H_2 at high temperatures, in Fig. 4 we show a comparison with close-coupling (CC) data calculated for 2000 K [76] and HITRAN data extrapolated to this temperature [102]. To estimate IR broadening coefficients from Raman Q-branch broadening data given in [76], the random-phase approximation (RPA) is used [103,104], assuming $\gamma_{J'\leftarrow J} \approx (\gamma_{J'\leftarrow J'} + \gamma_{J\leftarrow J})/2$, which should hold well at high temperatures where collisions mainly probe the region with short-range forces. The HITRAN data [102] are extrapolated to high temperatures using the provided single-power law coefficients.

All three theoretical calculations (CC, RB, and CRBM) predict a flat J-dependence of γ at high temperature except for the first couple of lines. The presence of strong m dependence in the HITRAN data stems from their use of the J-independent temperature coefficient n. Comparison of our calculations with CC results shows an absence of a pronounced drop between $|m| = 0$ and 1, as well as good agreement (for the best fit) between broadening coefficients everywhere else. This agreement is interesting in the sense that both the fitted CRBM predictions at room temperature (see Fig. 3) are nearly identical, while at $T = 2000$ K there is a significant difference. We believe this difference

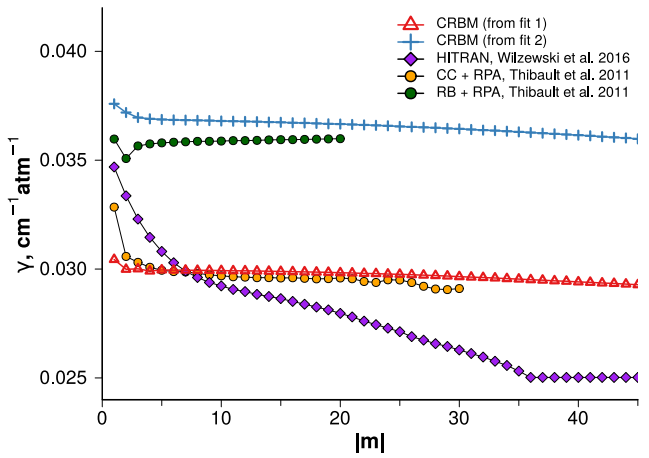

Fig. 4. C_2H_2–H_2 broadening coefficients at 2000 K. Data for comparison from [76,102] (see text).

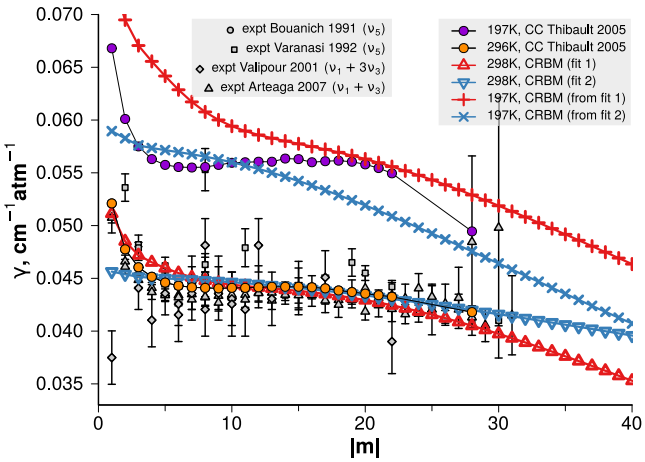

Fig. 5. He-broadening of acetylene at 197 K and room temperature. Experimental data from [17,26,28,40], theoretical data for comparison from [43].

is a consequence of the fitting procedure carried out just at room temperature, as well as the way we adjust the potential. Effectively, we are not fitting the potential itself, but the integral of cross-sections in Eq. (1), which depends parametrically on the potential, to get agreement with experimental broadening parameters at one temperature. To be more precise, for a given (b, v), a trajectory integral, which depends parametrically on the potential, is weighted by different factors in Eq. (1), notably by the (temperature-dependent) velocity distribution factor. Naturally, there can be different integrand functions that would give the same value of the integral at room temperature and very close broadening parameters. However, there is no guarantee that a weighted integral that gives good broadening parameters at one temperature will work well at others. In terms of fitting, this might represent multiple minima, where the 'correct' one is not necessarily global, or tighter constraints on the parameters' error bounds. To make the results more precise, a multi-temperature fit would be required, provided the experimental data are accurate and consistent. Otherwise, it will have the opposite effect.

Thus, although the potential itself does not depend on temperature, collisions at different velocities probe different regions of the potential, which makes the fit temperature-sensitive. Collisions with $b < \sigma_{\text{iso}}$ and low velocities cannot bring the molecules much closer than σ_{iso}, in contrast to high velocity collisions where the short-ranged features of the potential become predominant. In turn, low-velocity glancing collisions ($b \gg \sigma_{\text{iso}}$) are much more sensitive to the details of long-ranged interactions than high-velocity ones. When partial cross-sections for different velocities are weighted by the respective Maxwell–Boltzmann factors in Eq. (1) for a particular temperature, the quality of predictions might deteriorate if the desired temperature is very far from the one that served to fix the potential parameters. The final set of temperature-dependent broadening parameters has been generated using potential parameters from fit 1 because, although it performs slightly worse at room temperature, the agreement with CC/CS calculations at high temperature is much better.

3.1.2. C_2H_2–*He*

Helium broadening presents a tough case for the CRBM model. Because of a very shallow potential well and the absence of electric multipole interactions, the halfwidths end up extremely sensitive to the variation of the atom–atom parameters σ_{ij}, ε_{ij} for C–He and H–He. The initial estimate of the potential using helium parameters from [81] with Lorentz–Berthelot rules led to grossly overestimated results at 296 K ($\gamma(R(1)) = 0.099$ cm^{-1}atm^{-1}). The Waldman–Hagler combination rules [105] which showed excellent results for rare gas dimers led to more sensible but still overestimated predictions ($\gamma(R(1)) = 0.074$ cm^{-1}atm^{-1}). Fitting the potential parameters also presented difficulties, in part because of the large relative experimental errors which allowed deducing a number of J-dependent trends from wildly different atom–atom parameters.

By trial and error, we have identified several combinations of parameters that gave reasonable results, two of which are considered below. The first uses atom–atom contributions calculated with Waldman–Hagler rules as starting estimates, in conjunction with a fixed isotropic LJ potential taken from an *ab initio* study [106] that should give more or less realistic trajectories. The second one uses only those atom–atom parameters but with a more repulsive LJ 17-6 radial dependence in Eq. (7). The fit was performed for 95 experimental values of γ at room temperature with $|m| = 1, \ldots, 31$ taken from [17,26,28,40].

Results of calculations for the $\nu_1 + \nu_3$ band are shown in Fig. 5. At room temperature, both fits perform well, especially given the scatter in experimental data used during fitting, and the final rmse is again around 0.003 cm^{-1}atm^{-1} for both the fits. The agreement with the CC calculation is surprisingly good at intermediate J for both fits, with the first fit showing better agreement at small J and the second fit better following the results of quantum calculations at high J. Comparisons at low temperature do not allow one to determine the better fit because both perform poorly, which might be caused by the poor quality of the fitted interaction potential for low-energy collisions, or by the general deterioration of the semi-classical model predictions at low temperatures.

Nonetheless, we decided to keep the potential parameters from fit 2 because those predictions underestimated the broadening at small m, which is consistent with our room-temperature broadening calculation for H_2 and, as shown below, for other perturbers, too. This feature seems to be a systematic error of CRBM approach when applied to broadening of acetylene. Given that the non-conservation of rototranslational energy should not pose a problem for the C_2H_2–He system [43], and there are no electrostatic interactions between the molecules, further support is lent to the importance of line-coupling in S_2 matrices for acetylene.

3.1.3. C_2H_2–N_2

The results of CRBM calculation for nitrogen-broadening are shown in Fig. 6. The initial estimates for the potential parameters were taken from [33] (green line) and from combination rules [81] (violet line). We found that for nitrogen the fits performed poorly without an explicitly provided isotropic potential. For this reason, the isotropic potential parameters σ_{iso}, ε_{iso} were fixed (combination rules values from [81], *ab initio* values from [107]), which means only five parameters (two pairs of $\sigma_{ij}, \varepsilon_{ij}$, and θ) were used in the fitting procedure. Fitting

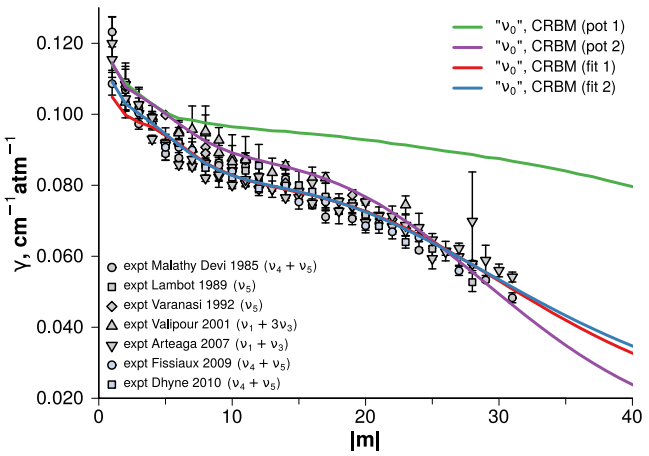

Fig. 6. C_2H_2–N_2 broadening parameters at room temperature with and without fitting. Experimental data for comparison from [17,26,28,31,32,36,37].

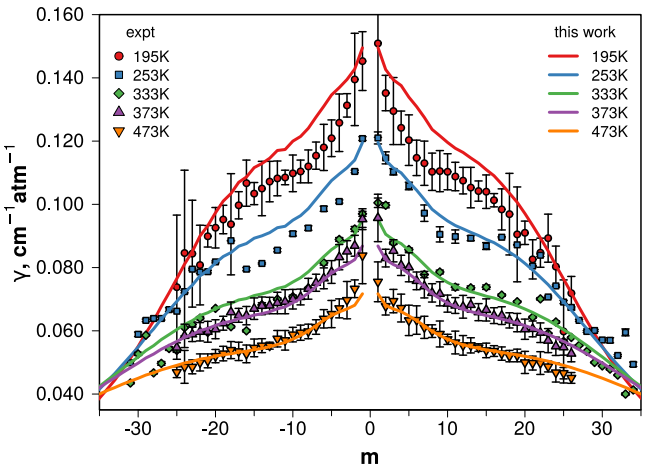

Fig. 7. Comparison of C_2H_2–N_2 halfwidth predictions from fit 1 with experimental data for the $\nu_1+\nu_3$ band not used in fitting, at 195, 373, 473 K [38] and 253, 333 K [45].

was performed based on the 157 experimental data for four bands: ν_5 [26,32], $(\nu_4+\nu_5)^0$ [31,36,37], $\nu_1+\nu_3$ [28], and $\nu_1+3\nu_3$ [17].

Unlike for hydrogen and helium broadening described above, the γ predictions with no fitting are markedly better, at least for some initial estimates. Otherwise, the same general J-dependent trend is observed as before – a gentle sloping and a slight underestimation of broadening for the first few lines.

Fig. 7 compares calculated values of γ from fit 1 with the experimental data [38,45] at five other temperatures which were not used in the fit. Experimental data is symmetric between R- and P-branches except for the first couple of lines; theoretical predictions do not show any significant difference between the branches. The overall agreement at 195 K is not great, most likely for the same reasons that were indicated in the helium discussion. At higher temperatures, the comparison gets progressively more favourable. Broadening of the first few lines is underestimated, as was the case for hydrogen. At the same time, at higher temperatures for $m > 20$ the theoretical trend seems to go above experimental data. This indicates that the fit struggles to constrain the short-range forces from more scarce high-J values of gamma. The situation could be improved by doing a multi-temperature fit or by including very high-J broadening parameters at room temperature that would be more sensitive to variations in those potential parameters. The quality of both fits 1 and 2 is comparable (0.0041 and 0.0036 $cm^{-1}atm^{-1}$), but we have chosen the first potential as slightly less repulsive and expect it to introduce a smaller error at higher temperatures.

3.1.4. C_2H_2–C_2H_2

Fitting was performed using 227 experimental values of γ with $|m| = 1,\ldots,36$ for seven different bands at room temperature taken from [12,14,17–19]. For this system it was essential to separately provide the isotropic potential instead of obtaining one from the expansion. In our fits we discovered that for a system with two long molecules and mean-field trajectories, the only relevant part of the atom–atom potential was the repulsion along the longest dimension of the molecules, that is the repulsive H–H interactions. Broadening parameters were largely insensitive to variations in other potential parameters (with the exception of θ), which is likely an artefact appearing from model approximations. To the best of our knowledge, there is no *ab initio* potential for the acetylene dimer, so we cannot fix the isotropic potential parameters to a known value as was done for He and N_2. Because of this, the isotropic potential parameters were fitted, together with three pairs of atom–atom parameters and the quadrupole moment. The initial estimates for the isotropic parameters were taken from [81], and the rest were taken from [44].

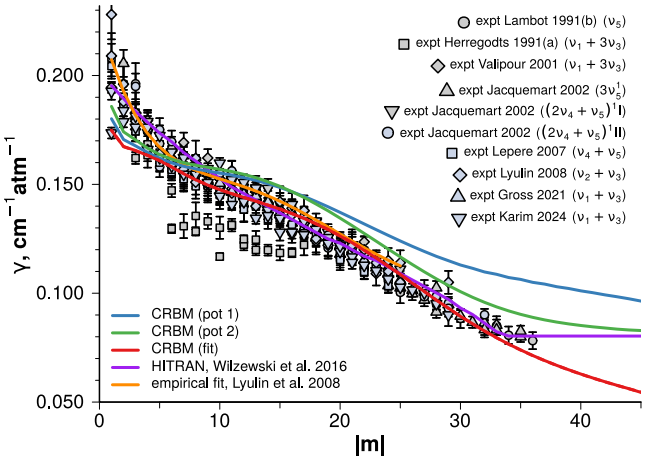

Fig. 8. Self-broadening of acetylene at room temperature. Data for comparison from [12,14,15,17–19,22,102,108].

Results of self-broadening parameters calculations at room temperature are shown in Fig. 8 and compared with experimental data [12,14,15,17–19,22,108] and some of the existing parametrizations [19,102]. Theoretical values of γ obtained with existing potential parameters from [14,44] are shown as a blue and a green curve, respectively. The former resembles the original RB calculation performed in that paper with the same set of potential parameters, while for the latter the comparison is not straightforward because a different trajectory model was used. The result of the calculation with the adjusted potential is depicted by a red curve in Fig. 8 which shows a significant improvement at middle and high values of the rotational index m. At small m, however, broadening coefficients are underestimated as was also observed for other molecules. The rmse of the fitted data was 0.0091 cm^{-1} and most of this error comes from lines with $|m| < 5$. Two empirical sets of data [19,102] obtained using Padé approximants are also shown for comparison.

3.1.5. C_2H_2–CO_2

Fitting was performed using 74 room-temperature experimental points from [35,41,42] with $|m| = 1,\ldots,31$ for three different bands. For this system, there are four pairs of atom–atom interactions. The initial estimates for O–H and C–O interactions were taken from [83], while C–C and H–C were taken from the self-broadening case. As with self-broadening, the isotropic potential was also provided in the model, and

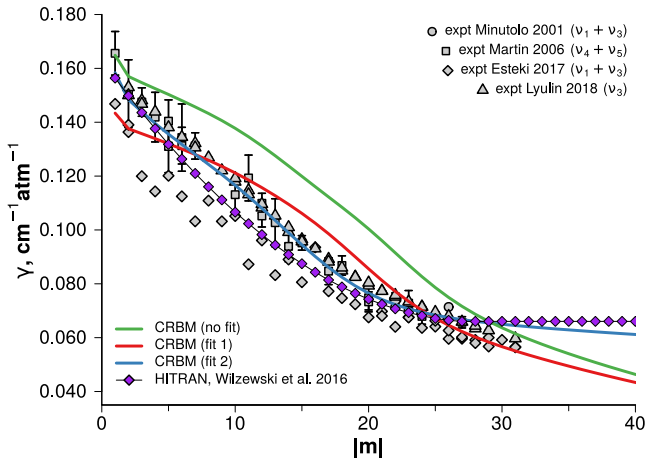

Fig. 9. C_2H_2–CO_2 broadening coefficients at room temperature. Data for comparison from [35,41,42,102].

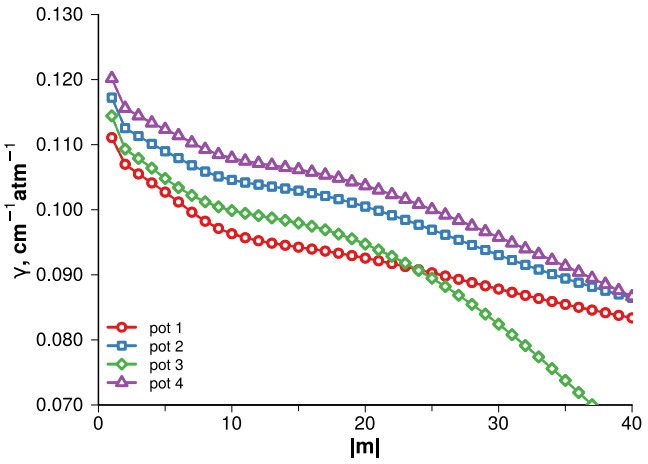

Fig. 10. Calculated C_2H_2–CO broadening coefficients at room temperature.

its parameters were constructed using Lorentz–Berthelot combination rules. The values for the acetylene dimer were taken from [81], while those for carbon dioxide dimer were obtained from fitting the *ab initio* data [109] to the 12-6 LJ form by fixing the repulsive wall position and the potential energy minimum.

Calculated line broadening parameters for C_2H_2 perturbed by CO_2 at room temperature are illustrated in Fig. 9 and compared with experimental data [35,41,42,47] and HITRAN data [102]. Note that the declared errors in [42,47] are too small to be seen on this plot. Theoretical predictions without fitting are overestimated over the entire range of $|m|$. In fit 1, the isotropic potential was fixed at the initial estimate to try and reduce the number of fitting variables, while in fit 2 all 11 parameters were being fitted. The rmse for fits 1 and 2 is, respectively, 0.0083 and 0.0032 $cm^{-1}atm^{-1}$. The second fit performs significantly better at all values of J except at highest values where theoretical values start to flatten out faster than the experimental ones. Despite that, we still use fit 2 to generate the final broadening parameters for all temperatures because fit 1 was obtained with some aggressive fitting of the quadrupole moment which we consider suspicious.

3.1.6. C_2H_2–CO

A recent study by Hu et al. [110] provides strong evidence for a CO and CO_2-rich atmosphere produced by magma outgassing in a hot exoplanet 55 Cancri e. In such conditions, line-broadening of minor species by carbon monoxide would play an important role on the observed spectrum. At the same time, to the best of our knowledge no experimental data on CO-broadening of acetylene are available in the literature. We therefore present the line-broadening calculation results without fitting the potential. Fig. 10 shows calculation results for four model potentials. The first one uses atom–atom parameters and θ from fitted C_2H_2–CO_2 with isotropic potential estimated from polarizabilities, and shows the smallest broadening coefficients. Potential two uses literature data for the atom–atom parameters [44,83], a higher value of $\theta = 4.5$ DÅ and the same isotropic potential for trajectories. Potential three and four differ from the second one by using different isotropic potentials for trajectories: potential three uses an expansion based on atom–atom parameters, while potential four uses values from Hirschfelder et al. [81] instead. All show similar J-dependence trends, except for potential 3; without either experimental data or a good potential, it is hard to improve the present results of modelling. We chose potential 2 to produce the reference temperature-dependent line-broadening coefficients as it represents the "middle ground" between different predictions. Comparing these results to other broadeners, hydrogen-broadening after fitting is slightly smaller, as is nitrogen and helium, while heavier C_2H_2 and CO_2 show larger broadening values due to more closely spaced rotational levels, even though they lack the dipole moment that CO possesses.

3.1.7. Vibrational dependence of γ (or lack thereof)

The typical influence of vibrational effects on acetylene's theoretical values of γ can be illustrated using the nitrogen-broadening as an example, for which there are sufficient experimental data on several vibrational bands. Previous experimental studies note that the vibrational contribution to halfwidths in acetylene seems to be small [12,13,17,28,29,111] as measured broadening coefficients for different bands lie within the uncertainties of those experiments. Still, it was important to check whether theoretical values for different bands would provide close predictions within experimental error bars, and if so, how different would values of γ be for bands with high number of excitations.

Calculations of γ for different bands are based on fits that use different S_1 contributions. As outlined above, the difference comes from approximations used in the calculation of dispersion interaction energy from known (ro)vibrational values of polarizability. For lines with $|m| > 30$, our values of the polarizability were extrapolated using a quadratic function in J which worked well for states with a low number of vibrational quanta, but not for $\nu_1 + 3\nu_3$, as Fig. 18 shows that the J-dependence is clearly not quadratic. Using such a poor fit leads to unphysically large S_1 term at very large Js, and since in the *Complex* RBM approach the S_1 and S_2 terms each affect both widths and shifts [82], even the halfwidths show an erroneous increase. To avoid this, and because rotational changes to interaction potential are smaller than the already small vibrational ones, we ultimately decided to work with $\bar{\alpha}_{v,J=0}$ in all our calculations. This choice had no impact on broadening parameters of other bands considered here.

Values γ for four bands calculated using our values of polarizability and the London formula Eq. (11) are presented in Fig. 11. These results show no significant vibrational dependence of broadening coefficients up to high J; at $|m| = 30$, the difference between the largest and smallest values (bands ν_5 and $\nu_1 + 3\nu_3$) is about $\Delta\gamma \approx 0.002$ $cm^{-1}atm^{-1}$. Similar results have been obtained when we used other methods of calculating dispersion interactions. We stress that such minor changes are not always the case, and imaginary terms in the exponent (S_1 and $\mathrm{Im}S_2$ in Eq. (2)) are known to influence halfwidths if collisions are weak [82].

Within each band, the predicted difference in γ between P- and R-branches is found to be negligible for all the lines except the first couple of lines in the ν_5 band. This is illustrated in Fig. 11, where P- and R-branches are shown as dashed and solid lines, respectively. This discrepancy for the ν_5 band is not caused by the S_1, but by the S_2 term.

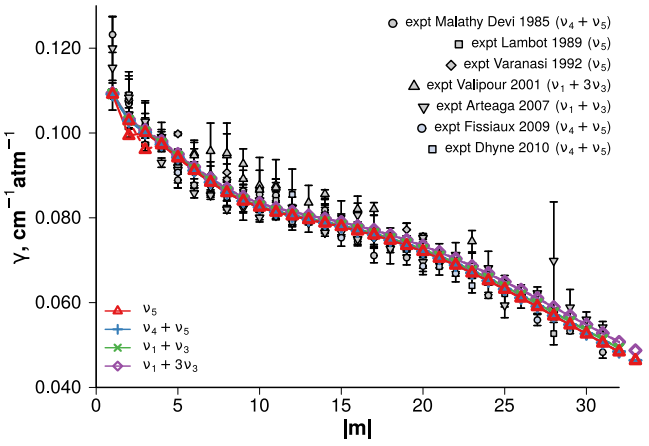

Fig. 11. C_2H_2–N_2 with predictions for several vibrational bands. R- and P-branches for the ν_5 band are shown in solid and dashed lines.

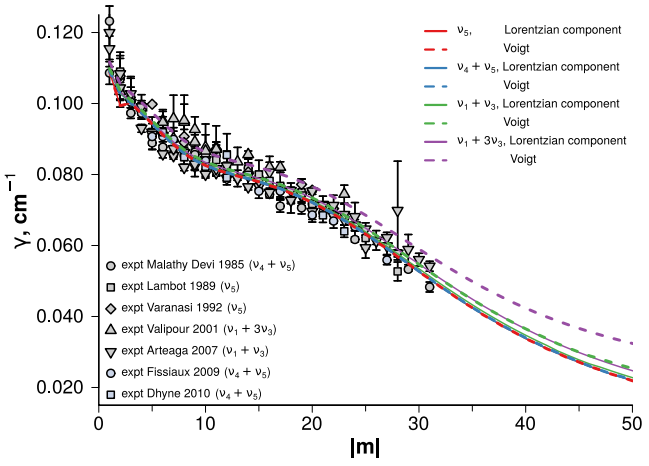

Fig. 12. Lorentzian and Voigt broadening parameters for C_2H_2–N_2 at room temperature and 1 atm. Voigt function calculated using [112].

This is a consequence of the interaction potential symmetry: when the two interacting molecules have an inversion centre, all odd ranks $l_{a,b}$ in Eq. (8) vanish and only collisional transitions with even ΔJ are allowed. Because $J = 0$ in the upper state does not exist, R(2) line of the ν_5 fundamental is missing a relaxation channel compared to other bands, so is the P(3) line. In our calculations, this effect is only present for the first few lines meaning the collisional transitions with $|\Delta J| > 4$ are much less likely. Calculations with a higher cutoff of short-ranged interactions $l_{\max} = 8$ did not change the picture significantly, which means that for the potentials considered terms with $l > 4$ are small, and our rank truncation in these calculations is justified. Accounting for of hexadecapole moments in the long-ranged forces is unlikely to change the picture at small $|m|$ values. Calculations using other treatments of the vibrationally-dependent potential mentioned above produced similar broadening coefficients.

At the same time, we note that our treatment of S_2 is not rigorous, in particular the reduced matrix elements are calculated with rigid rotor wavefunctions. If one used accurate linear molecule wavefunctions that allow for bending, this feature will likely change.

The absence of predicted vibrational dependence of broadening parameters is even more surprising for the case of self-broadening of acetylene. For instance, self-broadening of water is known to show a weak, but not negligible vibrational dependence of γ ($\sim$ 10%) [68], and for self-broadening in ammonia the differences between various bands vary several-fold [113]. For a species with no dipole moment, like carbon dioxide, self-broadening also showed vibrational dependence [114], albeit small. While acetylene also has no permanent dipole moment, the experimental self-broadening data for this molecule measured for 15 hot bands [13] show large scatter and suggest such a dependence might be present. Despite this, our calculations do not show any noticeable changes coming from the leading vibrational contribution, S_1, into the total scattering matrix in Eq. (1) when calculations are done for different bands.

Most software packages used to produce cross-sections for exoplanetary research work with the Voigt profile (describing the combined effect of collisional and Doppler broadening) and require γ_L and temperature as inputs. Considering the results above, it is safe to use vibrationally-independent values of γ_L for all bands of acetylene, and any substantial differences in broadening parameters between the bands is more likely to come from the frequency-dependent Doppler broadening contribution γ_D. Fig. 12 shows the purely Lorentzian contribution and the total broadening using the Voigt profile with the Doppler component calculated at room temperature as $\gamma_D \approx 3.581 \cdot 10^{-7}\omega_{fi}\sqrt{T/M}$ cm^{-1}, where M is molecular mass of the radiating molecule in Daltons. For bands with low vibrational excitation there is virtually no difference in $\gamma(m)$ and the lines on the plot overlap, but as one moves to higher excitations (centred at $\approx$ 6550 and 12750 cm^{-1}), the Doppler component brings a more significant contribution to the overall Voigt halfwidths. This is especially pronounced for higher J, where the Lorentzian components are small, as comparison of solid and dashed violet lines in Fig. 12 shows.

3.2. Line-shifting coefficients

Line shifts are obtained from our CRBM calculation as the imaginary part of Eq. (1). This quantity is known to be much more sensitive to the vibrational effects than broadening coefficients. In general, the quality of our line shift predictions for acetylene are worse than for broadening coefficients. Below we only discuss the cases of line-shifting by hydrogen and nitrogen calculated using polarizabilities taken from two different sources and different ways of estimating the vibrationally-dependent part of the potential. Possible reasons for discrepancies with the experiments and comparisons with other semi-classical calculations are considered in the discussions.

The pressure shifts of C_2H_2 by H_2 for $\nu_1 + \nu_3$ and ν_5 bands at room temperature are shown in Fig. 13, where we compare our theoretical results with the experimental values [27,28]. Solid lines are calculations using values of polarizability from this work, and dashed lines use the values from Russell and Spackman [55]. Both calculations use the London expression for the dispersion interaction, Eq. (11). It should be noted that the line shift calculations do not involve any additional fitting parameters beyond those used to model the line widths, and the vibrational variation of the theoretical shifts is mainly due to the variation of the electric polarizability $\bar{\alpha}_{v,J}$. With different sources for polarizability, the results end up quite different but in line with the polarizability differences between vibrationally excited and ground states $\bar{\alpha}_{v,J} - \bar{\alpha}_{gs,J}$ (see Fig. 18 below). Our predictions yield more negative values of the shifting coefficient than the experiment predicts, and, for hydrogen-shifting, show little to no J-dependence. Variations of the isotropic potential driving the trajectories do not change this picture, and no combination of S_1 expressions and values of $\bar{\alpha}$ led to us reproducing the observed small positive line shift values for the ν_5 band [27], which are highlighted on the figure.

The experimental data on the line shifts of C_2H_2 with N_2 are represented by four vibrational bands, ν_5 [27], $\nu_4+\nu_5$ [37], $\nu_1+\nu_3$ [28], and $\nu_1 + 3\nu_3$ [17], which allows for better evaluation of the vibrational effects and their importance in the CRBM model. From Fig. 1, the polarizabilities of these four states increase in order ν_5, $\nu_1 + \nu_3$, $\nu_4 + \nu_5$, and $\nu_1 + 3\nu_3$, and so do the line shift predictions for different bands. As shown in Fig. 14, the line shifts in transitions involving bending modes (orange and red points) are again significantly more negative

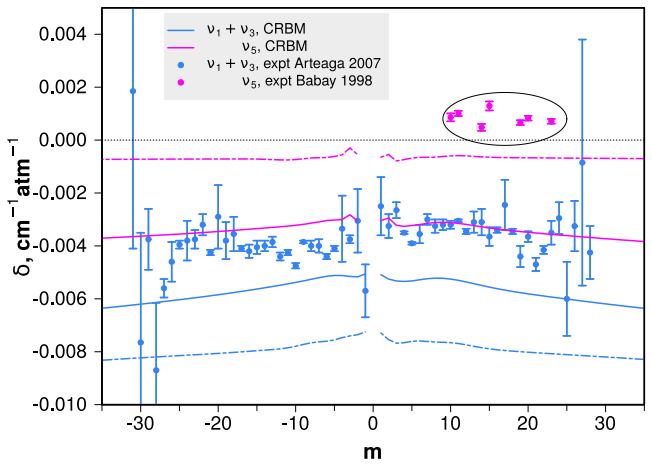

Fig. 13. H_2-shifting of acetylene at room temperature. Calculations shown in solid lines use polarizability from this work, those shown with a dashed line use polarizability from Russell and Spackman [55].

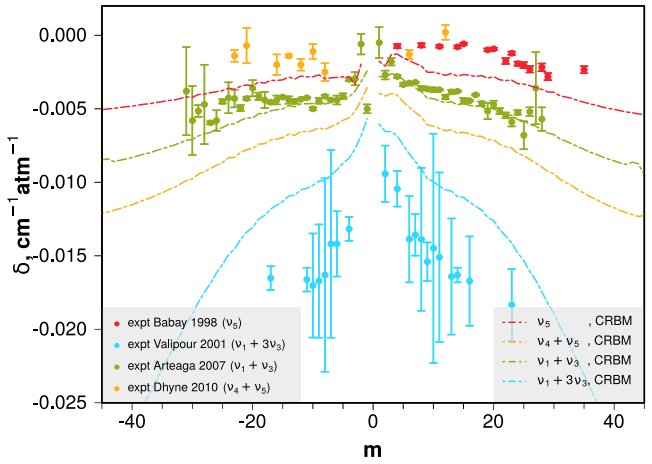

Fig. 14. Line-shifting coefficient of acetylene by N_2 calculated using polarizabilities from this work and the London expression for C_6.

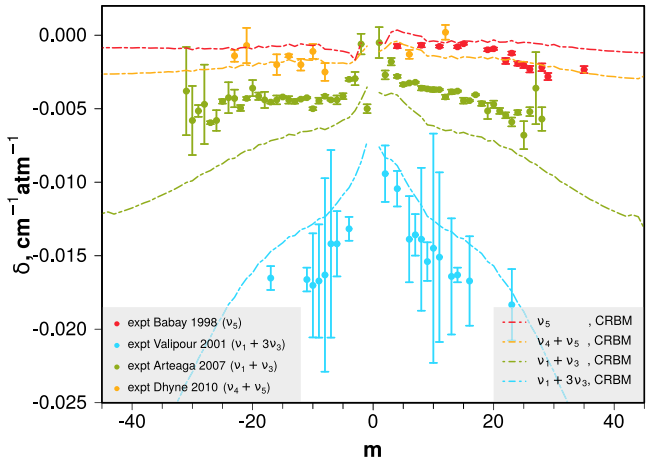

Fig. 15. Line-shifting coefficient of acetylene by N_2 calculated using polarizabilities from [55] and the London expression for C_6.

than the experiment. For the band with four quanta of stretch $\nu_1 + 3\nu_3$ (light blue), the theoretical shifts are smaller than experimentally measured ones. Although the $\nu_1 + \nu_3$ band fortuitously shows good agreement, still the trend in its P-branch shows a slightly different slope to the observed one. Because for this perturber J-dependence is more pronounced, it is also worth mentioning that with J-dependent polarizability values $\bar{\alpha}_{v,J\neq 0}$, the asymptotic R-branch line shifts ($m > 25$) are slightly lower than their P-branch counterparts. This is the result of rotation-vibrational coupling [115] introduced in the isotropic potential in S_1 from the use of *ab initio* wavefunctions in polarizability calculations. However, this effect seems to be very weak for acetylene ($\Delta\delta \approx 10^{-4}$ cm^{-1}atm^{-1}).

A different trend is obtained when using polarizabilities from Russell and Spackman [55] in calculations of S_1 and line-shifting coefficients as shown in Fig. 15. Here, the discrepancy between bending modes in theory and the experiment is reduced, so those theoretical values are small and close to zero. However, the calculated line shifts involving bands with stretching modes are more negative than with our values of α and still do not agree with the experimental data. Therefore, the quality of theoretical predictions remains only qualitative for any choice of polarizability data.

3.3. Parametrization of temperature dependence

The dependence of broadening parameters for different lines is considered as a function of temperature. Because vibrational dependence in S_1 is shown to be small, and that in the S_2 term is considered only partially, the widths of P(J) and R(J+1) lines are almost equal, and so the parametrization of γ vs $|m|$ should be sufficient to describe all the lines in our results. Two expressions are considered. The single-power law (SPL) is the one commonly used and is given by

$$\gamma(T) = \gamma_0 \left(\frac{T_{\rm ref}}{T}\right)^n, \tag{18}$$

where $\gamma_0 = \gamma(T_{\rm ref})$ is the line width parameter (half-width-at-half-maximum or HWHM), n is the temperature exponent and $T_{\rm ref}$ is the reference temperature usually selected to be 296 K. Another, more recently proposed parametrization is the double-power law (DPL) [116], which reads

$$\gamma(T) = c_1 \left(\frac{T_{\rm ref}}{T}\right)^{n_1} + c_2 \left(\frac{T_{\rm ref}}{T}\right)^{n_2}. \tag{19}$$

While for some transitions and certain collision systems SPL may be accurate within a couple hundred degrees, DPL has been shown to work better in larger temperature ranges for both semi-classical [83] and fully quantum calculations [117]. A similar expression for line shifts enables describing lines where the sign of lineshifts changes with temperature. However, because the agreement of line-broadening coefficients with experimental data is much better than that of lineshifts, here we only consider parametrization of broadening parameters.

To perform parametrization of our theoretical values, CRBM calculations have been performed for 14 temperatures from 200 to 3500 K, and the values of γ were then fitted using Eqs. (18) and (19). The temperature coefficient n in SPL was obtained by the least-squares fitting those data to Eq. (18). Indeed, in double logarithmic scale theoretical predictions should lie along a straight line if the single-power law holds. The double-power law which has four parameters (c_1, c_2, n_1, and n_2) requires the use of nonlinear least-squares fits. The SPL parameters γ_0 and n of C_2H_2 for all perturbers considered are provided in the form .broad files as part of the ExoMol diet [118] at www.exomol.com. See also the ExoMol 2024 release paper [70], where the recent updates of the ExoMol diet were presented. The SPL parameters are also provided as part of the supplementary material to this paper.

The function in Eq. (19) is not well-defined for nonlinear minimization routines because it might converge to local minima if during the iterations it approaches $c_{1,2} \to 0$ or $n_1 \to n_2$, where DPL reduces to SPL. To prevent the minimizer from exploring those regions of parameter space, the objective function is penalized as follows. In addition to the residuals $\gamma_{\rm CRBM} - \gamma_{\rm DPL}$ that enter the sum of squares for each

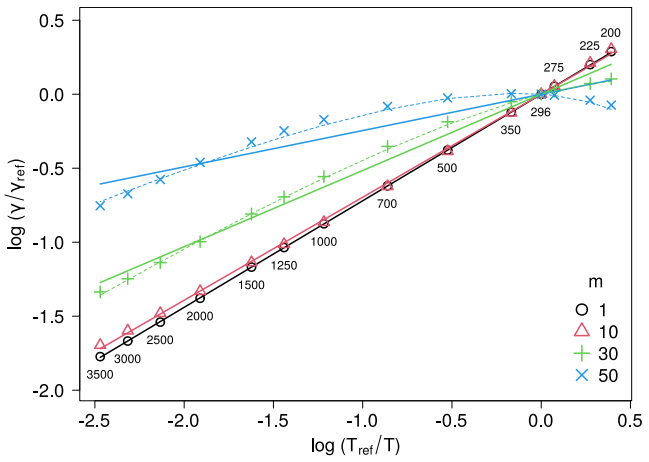

Fig. 16. Temperature dependence of broadening parameters for four self-broadened lines of acetylene from 200 to 3500 K. Points are calculated data, solid lines are linear regressions of those data representing the single-power law from Eq. (18), dashed lines are double-power law fits from Eq. (19).

temperature, we add three more terms $w_i \log|x_i|$, $x_i = c_{1,2}, n_1 - n_2$ that discourage the minimizer from converging to solutions with small values of x_i. The weights w_i are chosen such that for the initial estimates these three residuals are a few orders of magnitude smaller than those coming from halfwidth differences. For the first line $|m| = 1$, the initial estimates of parameters c_1 and n_1 are taken from the SPL results, and those for c_2 and n_2 are taken as fractions of the other two, i.e. $c_1/5$. The initial estimates for other lines are taken from solutions for the adjacent line $|m| - 1$. Although this procedure does not eliminate parameter correlation, it helps homogenize the variation of DPL parameters vs m and promotes their smooth variation.

Fig. 16 shows temperature dependence of broadening coefficients for four self-broadened acetylene lines in a double logarithmic scale (see Eq. (18)). The usual reference temperature of 296 K was chosen, which is where all the data pass through. For this system, broadening parameters of lines with small values of $|m|$ lie along straight lines and so can well be described by a single power law. Transitions between more excited rotational states clearly deviate from this behaviour and show the failure of the SPL description. DPL parametrization, shown for $m = 30, 50$ as a dashed line, give a much better representation of the data. This situation is also illustrated in normal scale in Fig. 17 for three self-broadened lines which also show DPL predictions as a better way to parametrize temperature dependence.

From a practical point of view, however, the advantages of the double-power law parametrization are minimal in this particular case. The largest deviations with SPL, as shown on Fig. 17, happen for intermediate ms at low temperatures and for high ms at all temperatures. At the same time, our low-temperature predictions are not too accurate, and broadening coefficients at high J are already small in magnitude. For completeness, we provide both parametrization in ExoMol's .broad files as m0 (SPL) and m2 (DPL) diets which can be found on the ExoMol website and the supplementary material.

4. Discussion

4.1. Broadening coefficients and fitting of the potential

The results of the calculations above show that using literature data for the atom–atom parameters and the electric multipoles lead to overestimated values of broadening parameters, which is especially pronounced for light perturbers, H_2 and He, that more strongly probe the repulsive wall of the potential during collisions. For heavier perturbing molecules, the literature data can be used as a first estimate. Fitting the potential parameters to the existing experimental line-broadening data helps improve the agreement, but for all the perturbers considered here the calculated broadening values at small m are underestimated after fitting.

One might ask whether it is possible to further tweak this "effective" potential to improve agreement with the experiment, in line with what was done, for example, in [45]. It is known [85,119], that lines with large halfwidths are more sensitive to long-range parameters and insensitive to atom–atom LJ parameters, so changing the long-range forces could improve agreement for small m. For example, in [33] this was done through modification of dispersion forces, and in [45] different values for perturber's θ were tested. In our fits, we found that the most effective way of increasing the broadening at small $|m|$ was to adjust electrostatic terms, but we had to use a smaller value of the quadrupole θ for acetylene to improve the overall agreement. This is also generally known [18], and semi-classical line shape calculations for molecules with large dipole or quadrupole moments often end up overestimated if literature data for electrostatic constants is used. For instance, the quadrupole moment of acetylene in a recent theoretical study is estimated to be within $\theta = 4.8{-}5.1$ DÅ [53] while in broadening calculations lower values led to best agreement: $\theta = 4.75$ [25], 4.5 [18], 4.0 [14], and even as low as 3.75 DÅ [33]. In our calculations from Fig. 3, the fits converged for the quadrupole moment values of 3.71 and 3.77 DÅ, respectively. Because changing this optimal parameter to improve predictions at small m would make the results worse everywhere else, no further manipulations were performed.

At the same time, there are preliminary results suggesting that reducing the quadrupole moment has a similar effect on broadening parameters as does the inclusion of line-coupling effects. Therefore, using a better theory could improve the solution of the inverse problem and produce better line shape parameters using more realistic quadrupole moment values. This will be investigated in a future paper, and for now we stick with the best solution obtained within CRBM. Despite certain shortcomings, the current fitting procedure leads to cancellation of errors coming from poor knowledge of the potential and certain approximations in the present level of theory, and thus enables capturing the general trends of experimentally observed broadening coefficients.

4.2. Calculation of expectation values for the isotropic polarizabilities

Table 2 presents a measure of zero-point corrections to polarizability $\Delta\bar{\alpha}_{\rm ZPC}$. Although this quantity is used by different authors in different meanings, we will still try to use it as a point of comparison. The study by Russell and Spackman [55] provides an expression for an arbitrary rovibrational expectation value of the polarizability of C_2H_2. Compared to their values, our $\Delta\bar{\alpha}_{v,J=0}$ is larger. The approaches to get those values, however, are quite different. In [55], the expectation values are calculated by expanding the isotropic polarizability surface in a Taylor series in normal mode coordinates. The expectation value expression for specific states is obtained using contact transformations and requires as inputs harmonic vibrational frequencies and various normal-mode coordinate derivatives of the energy and polarizability surfaces. In contrast, our calculations use polarizability expansion in linearized coordinates, and the expectation value is calculated in a straightforward fashion as an integral with variationally obtained rovibrational wavefunctions.

Comparisons of $\bar{\alpha}_{vJ}$ from our work and from Russell and Spackman [55] for other rovibrational states is presented in Fig. 18. In both cases, the change with rotational state is very small compared to that between vibrational states, which is not unexpected. Polarizability is often treated as a "volume" measure of a molecule, and changes in rotational state only slightly change bond lengths through centrifugal distortion terms, while the difference between different vibrational modes is much more pronounced. As for the vibrational states, the data show significant differences. This is especially concerning for the

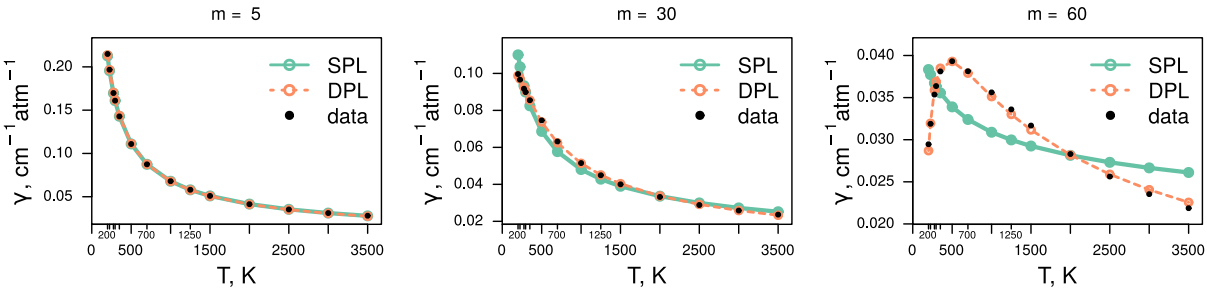

Fig. 17. Temperature dependence of broadening parameters for three self-broadened lines of acetylene. Points are calculated data, lines are SPL (Eq. (18)) and DPL (Eq. (19)) fits of calculated data.

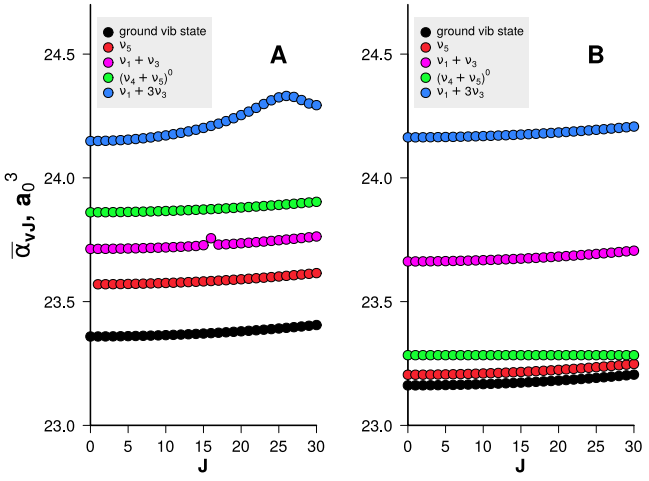

Fig. 18. Comparison of certain electronic polarizability expectation values between our results (A) and Russell and Spackman [55] (B).

ground vibrational state (black symbols) because both approaches use Taylor expansion about zero-field equilibrium geometry. One could expect the $\Delta\bar{\alpha}_{v,J=0}$ to be similarly displaced from α_e regardless of other computational details, but this is not the case. Another major difference is the relative contribution of bending motion to the polarizability (green and red symbols). Usually, the bending mode contribution to polarizability is smaller than for stretches as was shown for carbon dioxide [64] and water [120], and this trend was also observed for acetylene in a previous study [55].

We should note that Sharipov et al. [58] also consider vibrational averages of polarizabilities (their α^{UP}), including acetylene, but gives very different values for stretches and bendings that do not agree either with us or [55]. This is also the case for water data (compare with *ab initio* data from [120] or empirical estimates from [121]). Apparently, the choice of a simplified method which enabled covering a wide variety of species, cannot capture the finer details of vibrational dependence of polarizability, and thus we did not use these data in line shape calculations.

When it comes to vibrational contributions to the line broadening and shifts, it is not the absolute values, but their difference that appears in S_1 expressions. For this reason, the differences in $\bar{\alpha}_e$ do not matter as much as relative differences between the expectation values. We believe, that significant improvement of our polarizability expectation values could come from rectification of wavefunctions used to averaging the surface. Our current calculations were based on an approximated kinetic energy operator and a smaller basis set. An improvement of the wavefunctions might both lower the values of bending modes' averages and those of the ground-state through smaller zero-point contribution from ν_4 and ν_5 vibrations, which would also reflect on the line shift calculations.

We would like to emphasize that expectation values calculated in such a way include contributions from spontaneous resonances between different vibrational states in a polyad. An example of such a resonance can be seen in the lefthand panel of Fig. 18 appearing as an outlier of the $\nu_1 + \nu_3$ polarizability expectation values at $J = 16$.

Such polarizability calculations, in principle, can be carried out for any number of rovibrational states. However, assigning spectroscopic quantum numbers to those states is a tedious and often ambiguous process [122], so we have restricted our line shape calculations to a small number of states with well defined assignment. In order to minimize the amount of data, the vibrational dependence of polarizabilities is sometimes expressed as proportional to the number of quanta in different modes $\alpha_i = \alpha_0 + \sum_v c_i \cdot (v_i + d_i)$. Unfortunately, this simple form starts breaking down very quickly as the polyads are formed where the term "individual vibrational state" starts to lose its meaning. For example, the three states $(2\nu_4 + \nu_5)$ with different values of l_4, l_5, l_{tot} in Fig. 1 show quite different values of polarizabilities.

4.3. Line-shifting coefficients and their vibrational dependence

Effects of different vibrationally-dependent model potentials on line shifts as outlined in methodology are presented in Fig. 19 using C_2H_2–N_2 system as an example. Blue lines show calculated lineshift data for two bands, $\nu_1+\nu_3$ and $\nu_1+3\nu_3$, with the commonly used approach, where an extra vibrationally-dependent long-range isotropic potential is introduced. The respective C_6 coefficient is estimated from the London expression Eq. (11) using our values of polarizability.

Yellow lines show data where this potential also has a repulsive C_{12} contribution (estimated using [74]), and the C_6 is calculated using the Slater–Kirkwood expression Eq. (12). This expression gives a more attractive value of C_6, which for various states (and perturbers) is 30 to 50% times larger. For example, for the C_2H_2–N_2 dimer where acetylene is in the ground vibrational state, Eq. (11) gives $C_6 = 2.18\ E_h\text{Å}^6$ while with Eq. (12) one gets $3.26\ E_h\text{Å}^6$. This more attractive potential is reflected in more negative and spaced values of the lineshifts between different bands even when the repulsive C_{12} term is introduced.

Data shown by violet lines are calculated by scaling the existing isotropic potential instead of introducing a separate one for the purposes of S_1 calculation, and the scaling factors are based on expressions from [74] where C_6 is calculated using Eq. (11). These data show a different trend and as higher values of $|m|$ increase slightly before reaching asymptotic values. Nonetheless, none of the combinations lead to simultaneous agreement with all the experimental data sets. Modification of atom–atom parameters also do not lead to a significant improvement in shifts.

Unfortunately, these results fall short of representing the observed experimental trends for different vibrational bands. It is, therefore, interesting to compare our results to other semi-classical line shift data which show better agreement. There are multiple papers that modelled line shifts on a band-by-band basis. It is often done with a similar scaling of the isotropic potential [27,45,46]:

$$V_{\mathrm{iso}}^{\mathrm{modif}} = \frac{\Delta C_6}{C_6}\left[y\frac{C_{12}}{r^{12}} - \frac{C_6}{r^6}\right], \tag{20}$$

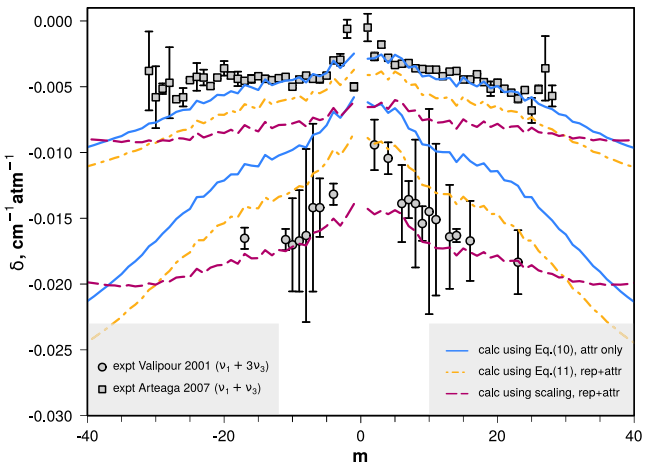

Fig. 19. Comparison of different approaches used in S_1 evaluation for the calculation of line-shifting coefficients for two different bands of acetylene in the C_2H_2–N_2 system.

Table 3
Comparison of parameters $\Delta C_6/C_6$ and y from Eq. (20) used to model vibrational dependence of the potential by various authors with values obtained from our polarizability calculations.

Data	Broadener	Band	$\Delta C_6/C_6$	y
From [27]	H_2	ν_5	0.010–0.015	5–6
Our calc (Eq. (11))			0.0090	1.674
(Eq. (12))			0.0069	1.886
From [27]	N_2	ν_5	0.010–0.015	0–1.5
Our calc (Eq. (11))			0.0090	1.549
(Eq. (12))			0.0065	1.756
From [45]		$\nu_1 + \nu_3$	0.005	0.7
Our calc (Eq. (11))			0.0152	1.552
(Eq. (12))			0.0109	1.760
From [46]	self	$3\nu_5$	0.006	1.6
Our calc (Eq. (11))			0.0264	1.440
(Eq. (12))			0.0197	1.586
From [46]		$(2\nu_4 + \nu_5)^1$ I	0.0045	0
Our calc (Eq. (11))			0.031	1.442
(Eq. (12))			0.023	1.588
From [46]		$(2\nu_4 + \nu_5)^1$ II	0.004	0.5
Our calc (Eq. (11))			0.027	1.441
(Eq. (12))			0.020	1.586

where the vibrational-state-dependent parameters are

$$\frac{\Delta C_6}{C_6} = \frac{\alpha_f - \alpha_i}{\alpha_i},$$

$$y = \frac{\Delta C_{12}/C_{12}}{\Delta C_6/C_6}.$$

The change in C_6 term can be tied to a (ro)vibrational change in polarizability, but usually the change in short-ranged forces is unknown. Often, both the parameters $\Delta C_6/C_6$ and y are treated as adjustable for that particular band. We would emphasize that both in our work and the ones cited above the atom–atom parameters, and thus, the trajectories, were fitted to obtain agreement with experimental line-broadening data. Additionally, in other works the coefficients $\Delta C_6/C_6$ and y were also fitted to adjust line shifts, while we used *ab initio* data for polarizabilities to estimate these vibrational changes in the interaction potential.

Table 3 compares the values of the vibrationally-dependent part of the potential for various perturbers and vibrational bands used in those works with our estimates. Based on our polarizability data, we present two scaling factors, one relying on London's expressions and the other — on the Slater–Kirkwood model. The C_{12} coefficient which appears in (20) twice, explicitly and in y, was estimated using the expression for the equilibrium separation r_m from [74].

Starting with shifting by H_2 in the ν_5 band [27], the values of the $\Delta C_6/C_6$ coefficient are comparable with our calculations, however, the second coefficient y is very different. To obtain agreement with line-shifting measurements in [27], modification of the short-ranged forces had to be much larger than what we predict based on the polarizability data alone. This also shows up in self-broadening data from [46], where the three bending bands have quite different y coefficients (1.6, 0, and 0.5), a variation not reflected in changes of acetylene average bond lengths or the isotropic polarizability. This might imply that although these fitting coefficients $\Delta C_6/C_6$ and y appear in the potential expression, such fitting also compensates for other aspects of theory.

Unfortunately, it is hard to pin down the exact reason here. The inability to predict positive lineshifts for H_2 and He probably comes from the too approximate repulsion term r^{-12}. The fact that shifts are influenced by the repulsive part of the potential was mentioned in [27] where C_2H_2 line shifts were also modelled for such perturbers as H_2, He, N_2, and Ar using the RB formalism. Vibrational dependence was approximated with the use of two parameters, $\Delta C_6/C_6$ and y which were adjusted to obtain agreement with their experimental lineshift data. The authors note that for heavy perturbers, in this case Ar and N_2, their model suggests that the long-range part of the vibrationally dependent isotropic potential is dominant, and the best agreement was obtained with a small value of $y \approx 0 - 1$, depending on $|m|$ within the band. The situation was completely different for light perturbers, H_2 and He, where to get positive line shifts, much greater importance had to be given to short-ranged interactions, $y \approx 4$ for He and $y \approx 5 - 6$ for H_2.

A different point was raised in fully classical studies of the broadening parameters [49]. The authors note that on average, trajectories driven by the isotropic potential, as done in CRBM, correspond to more distant turning points compared to the ones driven by the full potential. Using this line of reasoning from [27,49], the failure to predict shifts using vibrationally dependent model potentials might arise because in CRBM, the molecules during a collisional event never get close enough to experience the vibrational dependence of the potential at short range. At the same time, shifting the isotropic LJ parameters to allow for closer trajectories spoils the agreement of broadening parameters.

An indirect confirmation of the importance of short-ranged effects also comes from [119]. It was noted, that for self-broadening and shifting in water vapour, where interactions are strong and long-ranged, the largest contribution to the $Re(S_2)$ term is accumulated at larger distances, before the trajectories start to bend, and the trajectory model did not matter that much in that case. Same small differences between trajectory models were observed for line shifts which are determined by imaginary terms of S. However, for the two molecular pairs considered in this work, the longest ranged term is r^{-5} as opposed to r^{-3} in [119], so the details of the interaction potential at small intermolecular separations, as well as the trajectory intricacies, might become significant.

Probably a more important effect on line shifts is line-coupling. In a theoretical study on purely rotational lines of water [78] where the S_1 term does not appear, the account of line-coupling changed shifting coefficient of certain lines by as much as 25%. One can expect that for rovibrational lines of acetylene, where the S_1 terms are always present, this effect is even more important. Evaluation of the extent of this contribution is left for a future study.

5. Conclusions

A comprehensive computational study of line broadening and line shifts of C_2H_2 with a number of perturbers (H_2, He, N_2, C_2H_2, CO, and CO_2) is presented using the CRBM method. The interaction potentials were built following the usual CRBM protocol, with electrostatic and atom–atom parameters as its cornerstone. These input parameters are initially taken from the literature or from different studies and then refined by fitting to the experimental data on the line-broadening

coefficients. For C_2H_2 broadening, this protocol was found to yield reasonable agreement except for the lowest values of J which are underestimated.

Different models accounting for vibrational dependence of the potential during the collisional encounter have been tested. All of them rely on *ab initio* polarizability data of the radiating molecule calculated as expectation values in different vibrational states. All in all, no significant vibrational dependence of line broadening coefficients is observed, which is in agreement with the available experimental data. Neglecting rotational states in the S_1 matrix elements is shown to be valid as the effect of rotational dependence of the potential expressed through $\alpha = \alpha(J)$ is shown to be insignificant. For C_2H_2 line-shifting, poor agreement is observed.

The line shape parameters of acetylene resulting from this study are provided on www.exomol.com as part of the ExoMol C_2H_2 data. Rovibrational expectation values of the isotropic polarizability, as well as model potentials for the studies systems are provided as part of the supplementary material.

The CRBM methodology has proved to be robust, efficient and sufficiently accurate to be used for a large scale production of line broadening parameters for line lists containing up to billions of transitions especially for the molecules lacking the experimental information. An application of CRBM to other ExoMol molecules is currently underway.

CRediT authorship contribution statement

Andrei Sokolov: Writing – review & editing, Writing – original draft, Visualization, Validation, Software, Methodology, Investigation, Formal analysis, Conceptualization. **Sergei N. Yurchenko:** Writing – review & editing, Writing – original draft, Validation, Supervision, Software, Methodology, Investigation, Formal analysis, Conceptualization. **Jonathan Tennyson:** Writing – review & editing, Validation, Project administration, Methodology, Investigation, Funding acquisition, Formal analysis, Conceptualization. **Robert R. Gamache:** Writing – review & editing, Validation, Supervision, Software, Methodology, Investigation, Formal analysis, Conceptualization. **Bastien Vispoel:** Writing – review & editing, Validation, Software, Methodology, Investigation, Formal analysis, Conceptualization.

Declaration of competing interest

The authors declare that they have no known competing financial interests or personal relationships that could have appeared to influence the work reported in this paper.

Acknowledgements

This work used the DiRAC Data Intensive service DIaL2.5 at the University of Leicester, managed by the University of Leicester Research Computing Service on behalf of the STFC DiRAC HPC Facility (www.dirac.ac.uk). The DiRAC service at Leicester was funded by BEIS, UKRI and STFC capital funding and STFC operations grants. DiRAC is part of the UKRI Digital Research Infrastructure. This work was also supported by the European Research Council (ERC) under the European Union's Horizon 2020 research and innovation programme through Advance Grant number 883830. B. Vispoel would like to thank the F.R.S.-FNRS for postdoctoral financial support.

Appendix A. Supplementary data

The supplementary material contains (A) the expectation values of the isotropic polarizability obtained in this study, (B) the interaction potential parameters used for the calculation of line-broadening parameters, and (C) single- and double-power law coefficients obtained from fitting of the theoretical data.

Supplementary material related to this article can be found online at https://doi.org/10.1016/j.jqsrt.2024.109225.

Data availability

All data is provided within the article and the supplementary material.

References

[1] Pentsak EO, Murga MS, Ananikov VP. Role of acetylene in the chemical evolution of carbon complexity. ACS Earth Space Chem 2024. http://dx.doi.org/10.1021/acsearthspacechem.3c00223.

[2] Kanakidou M, Bonsang B, Roulley JCL, Lambert G, Martin D, Sennequier G. Marine source of atmospheric acetylene. Nature 1988;333:51–2. http://dx.doi.org/10.1038/333051a0.

[3] Zurek RW, Chicarro A, Allen MA, Bertaux JL, Clancy R, Daerden F, et al. Assessment of a 2016 mission concept: The search for trace gases in the atmosphere of Mars. Planet Space Sci 2011;59:284–91. http://dx.doi.org/10.1016/j.pss.2010.07.007.

[4] Villanueva GL, Mumma MJ, Novak RE, Radeva YL, Käufl HU, Smette A, et al. A sensitive search for organics (CH_4, CH_3OH, H_2CO, C_2H_6, C_2H_2, C_2H_4), hydroperoxyl (HO_2), nitrogen compounds (N_2O, NH_3, HCN) and chlorine species (HCl, CH_3Cl) on Mars using ground-based high-resolution infrared spectroscopy. Icarus 2013;223:11–27. http://dx.doi.org/10.1016/j.icarus.2012.11.013.

[5] Rinsland C, Baldacci A, Rao K. Acetylene bands observed in carbon stars - a laboratory study and an illustrative example of its application to IRC+10216. Astrophys J Suppl 1982;49:487–513. http://dx.doi.org/10.1086/190808.

[6] Giacobbe P, Brogi M, Gandhi S, Cubillos PE, Bonomo AS, Sozzetti A, et al. Five carbon- and nitrogen-bearing species in a hot giant planet's atmosphere. Nature 2021;592:205–8. http://dx.doi.org/10.1038/s41586-021-03381-x.

[7] Bergin EA, Kempton EMR, Hirschmann M, Bastelberger ST, Teal DJ, Blake GA, et al. Exoplanet volatile carbon content as a natural pathway for Haze formation. Astrophys J Lett 2023;949:L17. http://dx.doi.org/10.3847/2041-8213/acd377.

[8] Birkby JL. Spectroscopic direct detection of exoplanets. Cham: Springer International Publishing; 2018, p. 1485–508. http://dx.doi.org/10.1007/978-3-319-55333-7_16.

[9] Chubb KL, et al. Data availability and requirements relevant for the ariel space mission and other exoplanet atmosphere applications. RAS Tech Instr 2024.

[10] Fortney JJ, Robinson TD, Domagal-Goldman S, Genio ADD, Gordon IE, Gharib-Nezhad E, et al. The need for laboratory measurements and ab initio studies to aid understanding of exoplanetary atmospheres. 2019, arXiv:1905.07064.

[11] Gandhi S, Brogi M, Yurchenko SN, Tennyson J, Coles PA, Webb RK, et al. Molecular cross-sections for high-resolution spectroscopy of super-Earths, warm Neptunes, and hot Jupiters. Mon Not R Astron Soc 2020;495:224–37. http://dx.doi.org/10.1093/mnras/staa981.

[12] Jacquemart D, Mandin JY, Dana V, Régalia-Jarlot X, Von der Heyden P. Multispectrum fitting measurements of line parameters for 5-μm cold bands of acetylene. J Quant Spectrosc Radiat Transfer 2002;75:397–422. http://dx.doi.org/10.1016/S0022-4073(02)00017-1.

[13] Jacquemart D, Mandin JY, Dana V, Régalia-Jarlot JJ, Décatoire D, et al. The spectrum of acetylene in the 5-μm region from new line-parameter measurements. J Quant Spectrosc Radiat Transfer 2003;76:237–67. http://dx.doi.org/10.1016/S0022-4073(02)00055-9.

[14] Lambot D, Olivier A, Blanquet G, Walrand J, Bouanich JP. Diode-laser measurements of collisional line broadening in the ν_5 band of C_2H_2. J Quant Spectrosc Radiat Transfer 1991;45:145–55. http://dx.doi.org/10.1016/0022-4073(91)90004-A.

[15] Herregodts F, Hurtmans D, Auwera JVander, Herman M. Laser spectroscopy of the $\nu_1+3\nu_3$ absorption band in $^{12}C_2H_2$. I. Pressure broadening and absolute line intensity measurements. J Chem Phys 1999;111:7954–60. http://dx.doi.org/10.1063/1.480129.

[16] Herregodts F, Hepp M, Hurtmans D, Auwera J Vander, Herman M. Laser spectroscopy of the $\nu_1 + 3\nu_3$ absorption band in $^{12}C_2H_2$. II. Self-collisional lineshift measurements. J Chem Phys 1999;111:7961–5. http://dx.doi.org/10.1063/1.480130.

[17] Valipour H, Zimmermann D. Investigation of J dependence of line shift, line broadening, and line narrowing coefficients in the $\nu_1 + 3\nu_3$ absorption band of acetylene. J Chem Phys 2001;114:3535–45. http://dx.doi.org/10.1063/1.1333022.

[18] Lepère M, Blanquet G, Walrand J, Bouanich JP, Herman M, Auwera JV. Self-broadening coefficients and absolute line intensities in the $\nu_4 + \nu_5$ band of acetylene. J Mol Spectrosc 2007;242:25–30. http://dx.doi.org/10.1016/j.jms.2007.01.004.

[19] Lyulin OM, Jacquemart D, Lacome N, Perevalov VI, Mandin JY. Line parameters of acetylene in the 1.9 and 1.7μm spectral regions. J Quant Spectrosc Radiat Transfer 2008;109:1856–74. http://dx.doi.org/10.1016/j.jqsrt.2007.11.016.

[20] Povey C, Predoi-Cross DR. Line shape study of acetylene transitions in the $\nu_1+\nu_2+\nu_4+\nu_5$ band over a range of temperatures. J Mol Spectrosc 2011;268:177–88. http://dx.doi.org/10.1016/j.jms.2011.04.020.

[21] Sajid MB, Es-sebbar Et, Farooq A. Measurements of linestrengths, N_2-, Ar-, He- and self-broadening coefficients of acetylene in the $\nu_4 + \nu_5$ combination band using a cw quantum cascade laser. J Quant Spectrosc Radiat Transf 2014;148:1–12. http://dx.doi.org/10.1016/j.jqsrt.2014.06.014.

[22] Gross EC, Tsang KA, Sears TJ. Re-evaluation of ortho-para-dependence of self pressure-broadening in the $\nu_1 + \nu_3$ band of acetylene. J Chem Phys 2021;154:054305. http://dx.doi.org/10.1063/5.0036602.

[23] Okubo S, Iwakuni K, Kato H, Hong FL, Sasada H, Inaba H, et al. The pressure effect on the line profiles observed in the $\nu_1 + \nu_3$ band of acetylene: Revisited. J Mol Spectrosc 2023;396:111823. http://dx.doi.org/10.1016/j.jms.2023.111823.

[24] Blass WE, Chin VWL. Hydrogen and nitrogen broadening of the lines of C_2H_2 at 14 μm. J Quant Spectrosc Radiat Transfer 1987;38:185–8. http://dx.doi.org/10.1016/0022-4073(87)90084-7.

[25] Lambot D, Blanquet G, Walrand J, Bouanich JP. Diode-laser measurements of H_2-broadening coefficients in the ν_5 band of C_2H_2. J Mol Spectrosc 1991;150:164–72. http://dx.doi.org/10.1016/0022-2852(91)90199-K.

[26] Varanasi P. Intensity and linewidth measurements in the 13.7 μm fundamental bands of $^{12}C_2H_2$ and $^{12}C^{13}CH_2$ at planetary atmospheric temperatures. J Quant Spectrosc Radiat Transfer 1992;47:263–74. http://dx.doi.org/10.1016/0022-4073(92)90145-T.

[27] Babay A, Ibrahimi M, Lemaire V, Lemoine B, Rohart F, Bouanich JP. Line frequency shifting in the ν_5 band of C_2H_2. J Quant Spectrosc Radiat Transfer 1998;59:195–202. http://dx.doi.org/10.1016/S0022-4073(97)00122-2.

[28] Arteaga S, Bejger C, Gerecke J, Hardwick J, Martin Z, Mayo J, et al. Line broadening and shift coefficients of acetylene at 1550 nm. J Mol Spectrosc 2007;243:253–66. http://dx.doi.org/10.1016/j.jms.2007.04.007.

[29] Thibault F, Fuller E, Grabow K, Hardwick J, Marcus C, Marston D, et al. Experimental line broadening and line shift coefficients of the acetylene $\nu_1 + \nu_3$band pressurized by hydrogen and deuterium and comparison with calculations. J Mol Spectrosc 2009;256:17–27. http://dx.doi.org/10.1016/j.jms.2009.01.011.

[30] Varanasi P, Giver LP, Valero FPJ. Infrared absorption by acetylene in the 12–14 μm region at low temperatures. J Quant Spectrosc Radiat Transfer 1983;30:497–504. http://dx.doi.org/10.1016/0022-4073(83)90003-1.

[31] Devi V Malathy, Benner D Chris, Rinsland CP, Smith MAH, Sidney BD. Tunable diode laser measurements of N_2- and air-broadened halfwidths: Lines in the $(\nu_4 + \nu_5)^0$ band of $^{12}C_2H_2$ near 7.4 μm. J Mol Spectrosc 1985;114:49–53. http://dx.doi.org/10.1016/0022-2852(85)90335-2.

[32] Lambot D, Blanquet G, Bouanich JP. Diode laser measurements of collisional broadening in the ν_5 band of C_2H_2 perturbed by O_2 and N_2. J Mol Spectrosc 1989;136:86–92. http://dx.doi.org/10.1016/0022-2852(89)90221-X.

[33] Bouanich JP, Lambot D, Blanquet G, Walrand J. N_2- and O_2-broadening coefficients of C_2H_2 IR lines. J Mol Spectrosc 1990;140:195–213. http://dx.doi.org/10.1016/0022-2852(90)90134-C.

[34] Bouanich JP, Blanquet G, Walrand J. Line-mixing effects in He- and N_2-broadened $\Sigma \rightarrow \Pi$ infrared Q branches of C_2H_2. J Mol Spectrosc 2000;203:41–8. http://dx.doi.org/10.1006/jmsp.2000.8160.

[35] Minutolo P, Corsi C, D'Amato F, De Rosa M. Self- and foreign-broadening and shift coefficients for C_2H_2 lines at 1.54 μm. Eur Phys J D 2001;17:175–9. http://dx.doi.org/10.1007/s100530170020.

[36] Fissiaux L, Dhyne M, Lepère M. Diode-laser spectroscopy: Pressure dependence of N_2-broadening coefficients of lines in the band of C_2H_2. J Mol Spectrosc 2009;254:10–5. http://dx.doi.org/10.1016/j.jms.2008.12.003.

[37] Dhyne M, Joubert P, Populaire JC, Lepère M. Collisional broadening and shift coefficients of lines in the $\nu_4 + \nu_5$ band of $^{12}C_2H_2$ diluted in n_2 from low to room temperatures. J Quant Spectrosc Radiat Transfer 2010;111:973–89. http://dx.doi.org/10.1016/j.jqsrt.2009.12.004.

[38] Campbell N, Cook J, Coombs B, Fuller E, Hardwick J, Hurley S, et al. Temperature dependence of pressure broadening and shifts of acetylene at 1550 nm by N_2. Mol Phys 2011;109:2199–208. http://dx.doi.org/10.1080/00268976.2011.609139.

[39] Le T, Fissiaux L, Tran H, Lepère M. O_2-broadening coefficients of acetylene lines in the $\nu_4 + \nu_5$ band at room temperature. J Mol Spectrosc 2015;314:48–53. http://dx.doi.org/10.1016/j.jms.2015.06.003.

[40] Bouanich JP, Boulet C, Blanquet G, Walrand J, Lambot D. Lineshapes and broadening coefficients in the ν_5 band of C_2H_2 in collision with Kr and He. J Quant Spectrosc Radiat Transfer 1991;46:317–24. http://dx.doi.org/10.1016/0022-4073(91)90096-9.

[41] Martin B, Walrand J, Blanquet G, Bouanich JP, Lepère M. CO_2-broadening coefficients in the $\nu_4 + \nu_5$ band of acetylene. J Mol Spectrosc 2006;236:52–7. http://dx.doi.org/10.1016/j.jms.2005.12.011.

[42] Lyulin OM, Petrova TM, Solodov AM, Solodov AA, Perevalov VI. CO_2-broadening and shift coefficients in the ν_3 and $\nu_2+(\nu_4+\nu_5)^0_+$ bands of acetylene. J Quant Spectrosc Radiat Transfer 2018;208:96–100. http://dx.doi.org/10.1016/j.jqsrt.2017.12.029.

[43] F. Thibault. Theoretical He-broadening coefficients of infrared and Raman C_2H_2 lines and their temperature dependence. J Mol Spectrosc 2005;234:286–8. http://dx.doi.org/10.1016/j.jms.2005.09.008.

[44] Buldyreva J, Nguyen L. On the role of trajectory modelling in the C_2H_2 infrared line-broadening computation. Mol Phys 2004;102:1523–35. http://dx.doi.org/10.1080/00268970410001725837.

[45] Rozario H, Garber J, Povey C, Hurtmans D, Buldyreva J, Predoi-Cross A. Experimental and theoretical study of N_2-broadened acetylene line parameters in the $\nu_1 + \nu_3$ band over a range of temperatures. Mol Phys 2012;110:2645–63. http://dx.doi.org/10.1080/00268976.2012.720040.

[46] Galalou S, Aroui H. Theoretical self-broadening and self-shifting coefficients of $^{12}C_2H_2$ transitions in the $3\nu_5$, $(2\nu_4 + \nu_5)$I and $(2\nu_4 + \nu_5)$II bands. J Mol Spectrosc 2013;288:61–6. http://dx.doi.org/10.1016/j.jms.2013.04.007.

[47] Esteki K, Mashwood AA, Dudaryonok A, Buldyreva J, Predoi-Cross N, et al. Collisional line-shape parameters and their temperature dependence for the $\nu_1 + \nu_3$ band of C_2H_2 perturbed by CO_2. J Quant Spectrosc Radiat Transfer 2017;203:454–60. http://dx.doi.org/10.1016/j.jqsrt.2017.02.002.

[48] Ivanov S, Nguyen L, Buldyreva J. Comparative analysis of purely classical and semiclassical approaches to collision line broadening of polyatomic molecules: I. C_2H_2–Ar case. J Mol Spectrosc 2005;233:60–7. http://dx.doi.org/10.1016/j.jms.2005.05.014.

[49] Ivanov SV, Buzykin OG. Classical calculation of self-broadening in N_2 Raman spectra. Mol Phys 2008;106:1291–302. http://dx.doi.org/10.1080/00268970802270034.

[50] Ivanov SV, Buzykin OG. On the accuracy of classical, semiclassical and quantum methods in collision line broadening calculations: Comparative analysis for C_2H_2–Ar, He systems. J Quant Spectrosc Radiat Transfer 2010;111:2341–53. http://dx.doi.org/10.1016/j.jqsrt.2010.04.031.

[51] Robert D, Bonamy J. Short range force effects in semiclassical molecular line broadening calculations. J Physique 1979;40:923–43. http://dx.doi.org/10.1051/jphys:01979004010092300.

[52] Ma Q, Tipping R, Boulet C. Modification of the Robert–Bonamy formalism in calculating Lorentzian half-widths and shifts. J Quant Spectrosc Radiat Transfer 2007;103:588–96. http://dx.doi.org/10.1016/j.jqsrt.2006.08.001.

[53] Coccia E, Chernomor O, Barborini M, Sorella S, Guidoni L. Molecular electrical properties from quantum Monte Carlo Calculations: Application to ethyne. J Chem Theory Comput 2012;8:1952–62. http://dx.doi.org/10.1021/ct300171q.

[54] U. Hohm. Experimental static dipole–dipole polarizabilities of molecules. J Mol Struct 2013;1054–1055:282–92. http://dx.doi.org/10.1016/j.molstruc.2013.10.003.

[55] Russell AJ, Spackman MA. Accurate ab initio study of acetylene Vibrational and rotational corrections to electrical properties. Mol Phys 1996;88:1109–36. http://dx.doi.org/10.1080/00268979609484496.

[56] Handy NC, Pople JA, Head-Gordon K, Trucks GW. Size-consistent Brueckner theory limited to double substitutions. Chem Phys Lett 1989;164:185–92. http://dx.doi.org/10.1016/0009-2614(89)85013-4.

[57] Monten R, Hajgató B, Deleuze MS. Many-body calculations of molecular electric polarizabilities in asymptotically complete basis sets. Mol Phys 2011;109:2317–39. http://dx.doi.org/10.1080/00268976.2011.579580.

[58] Sharipov AS, Loukhovitski BI, Starik AM. The influence of vibrations of polyatomic molecules on dipole moment and static dipole polarizability: theoretical study. J Phys B: At Mol Opt Phys 2017;50:165101. http://dx.doi.org/10.1088/1361-6455/aa7f80.

[59] Yurchenko SN, Thiel W, Jensen P. Theoretical ROVibrational Energies (TROVE): A robust numerical approach to the calculation of rovibrational energies for polyatomic molecules. J Mol Spectrosc 2007;245:126–40. http://dx.doi.org/10.1016/j.jms.2007.07.009.

[60] Hartmann JM, Boulet C, Robert D. Collisional effects on molecular spectra: Laboratory experiments and models, consequences for applications. 1st ed. Elsevier Science; 2008, http://dx.doi.org/10.1016/B978-0-444-52017-3.X0001-5.

[61] Tsao C, Curnutte B. Line-widths of pressure-broadened spectral lines. J Quant Spectrosc Radiat Transfer 1962;2:41–91. http://dx.doi.org/10.1016/0022-4073(62)90013-4.

[62] R. Kubo. Generalized cumulant expansion method. J Phys Soc Japan 1962;17:1100–20. http://dx.doi.org/10.1143/JPSJ.17.1100.

[63] Ma Q, Boulet C, Tipping RH. Refinement of the Robert-Bonamy formalism: Considering effects from the line coupling. J Chem Phys 2013;139:034305. http://dx.doi.org/10.1063/1.4813234.

[64] Gamache RR, Lamouroux J, Laraia AL, Hartmann JM, Boulet C. Semiclassical calculations of half-widths and line shifts for transitions in the 30012←00001 and 30013←00001 bands of CO_2, I: Collisions with N_2. J Quant Spectrosc Radiat Transfer 2012;113:976–90. http://dx.doi.org/10.1016/j.jqsrt.2012.02.014.

[65] Ma Q, Tipping RH, Boulet C. Irreducible correlation functions of the $\hat{S}$ matrix in the coordinate representation: Application in calculating Lorentzian half-widths and shifts. J Chem Phys 2006;124:014109. http://dx.doi.org/10.1063/1.2139671.

[66] Rabitz HA, Gordon RG. Semiclassical perturbation theory of molecular collisions. I. First and second order. J Chem Phys 1970;53:1815–31. http://dx.doi.org/10.1063/1.1674259.

[67] Gray CG, Gubbins KE. Theory of Molecular Fluids: I: Fundamentals. In: International series of monographs on chemistry. Oxford: Oxford University Press; 1984, p. 644. http://dx.doi.org/10.1093/oso/9780198556022.001.0001.

[68] Gamache RR, Hartmann JM. Collisional parameters of H_2O lines: effects of vibration. J Quant Spectrosc Radiat Transfer 2004;83:119–47. http://dx.doi.org/10.1016/S0022-4073(02)00296-0.

[69] Ma Q, Tipping R, Boulet C, Thibault F, Bonamy J. Vibration-dependent trajectories and their effects on vibrational dephasing. J Mol Spectrosc 2007;243:105–12. http://dx.doi.org/10.1016/j.jms.2007.01.003.

[70] Tennyson J, Yurchenko SN, Zhang J, Bowesman CA, Brady RP, Buldyreva J, et al. The release of the ExoMol database: molecular line lists for exoplanet and other hot atmospheres. J Quant Spectrosc Radiat Transfer 2024;(2024):109083. http://dx.doi.org/10.1016/j.jqsrt.2024.109083.

[71] Gamache RR, Rey M, Vispoel B, Tyuterev VG. Reduced matrix elements for collisionally induced transitions of $^{12}CH_4$. J Quant Spectrosc Radiat Transfer 2019;235:31–9. http://dx.doi.org/10.1016/j.jqsrt.2019.06.010.

[72] A. Stone. The theory of intermolecular forces. Oxford University Press; 2013, http://dx.doi.org/10.1093/acprof:oso/9780199672394.001.0001.

[73] Johnson III RD. NIST computational chemistry comparison and benchmark database. 2022.

[74] Cambi R, Cappelletti D, Liuti G, Pirani F. Generalized correlations in terms of polarizability for van der Waals interaction potential parameter calculations. J Chem Phys 1991;95:1852–61. http://dx.doi.org/10.1063/1.461035.

[75] Thibault F, Martínez RZ, Bermejo D, Ivanov SV, Buzykin OG, Ma Q. An experimental and theoretical study of nitrogen-broadened acetylene lines. J Quant Spectrosc Radiat Transfer 2014;142:17–24. http://dx.doi.org/10.1016/j.jqsrt.2014.03.009.

[76] Thibault F, Ivanov SV, Buzykin OG, Gomez L, Dhyne M, Joubert P, et al. Comparison of classical, semiclassical and quantum methods in hydrogen broadening of acetylene lines. J Quant Spectrosc Radiat Transfer 2011;112:1429–37. http://dx.doi.org/10.1016/j.jqsrt.2011.02.011.

[77] Margottin-Maclou F, Henry A, Valentin A. Pressure-induced line shifts in the ν_3 band of nitrous oxide perturbed by N_2, O_2, He, Ar and Xe. J Quant Spectrosc Radiat Transfer 1996;56:1–16. http://dx.doi.org/10.1016/0022-4073(96)00029-5.

[78] Ma Q, Boulet C, Tipping RH. Effects on calculated half-widths and shifts from the line coupling for asymmetric-top molecules. J Chem Phys 2014;140:244301. http://dx.doi.org/10.1063/1.4883058.

[79] Ma Q, Boulet C. Branch dependence of halfwidths: Theoretical analysis of N_2-broadened halfwidths of CH_3Br in the ν_6 band. J Quant Spectrosc Radiat Transfer 2024;320:108972. http://dx.doi.org/10.1016/j.jqsrt.2024.108972.

[80] Buldyreva J, Lavrentieva N, Starikov V. Collisional line broadening and shifting of atmospheric gases. Imperial College Press; 2010, http://dx.doi.org/10.1142/p731.

[81] Hirschfelder JO, Curtiss CF, Bird RB. Molecular theory of gases and liquids. Corr. print. with notes added. J. Wiley & sons; 1964.

[82] Lynch R, Gamache RR, Neshyba SP. Fully complex implementation of the Robert–Bonamy formalism: Half widths and line shifts of H_2O broadened by N_2. J Chem Phys 1996;105(14):5711–21. http://dx.doi.org/10.1063/1.472416, http://aip.scitation.org/doi/10.1063/1.472416.

[83] Régalia L, Cousin E, Gamache R, Vispoel B, Robert S, Thomas X. Laboratory measurements and calculations of line shape parameters of the H_2O–CO_2 collision system. J Quant Spectrosc Radiat Transfer 2019;231:126–35. http://dx.doi.org/10.1016/j.jqsrt.2019.04.012.

[84] Bouanich J, Predoi-Cross A. Theoretical calculations for line-broadening and pressure-shifting in the $\nu_1+\nu_2+\nu_4+\nu_5$ band of acetylene over a range of temperatures. Mol Phys 2011;109:2071–81. http://dx.doi.org/10.1080/00268976.2011.599342.

[85] Ma Q, Tipping R, Gamache R. Uncertainties associated with theoretically calculated N_2-broadened half-widths of H_2O lines. Mol Phys 2010;108:2225–52. http://dx.doi.org/10.1080/00268976.2010.505209.

[86] Lucchesini A, Rosa MDe, Pelliccia D, Ciucci A, Gabbanini C, Gozzini S. Diode laser spectroscopy of overtone bands of acetylene. Appl Phys B 1996;63:277–82. http://dx.doi.org/10.1007/BF01833797.

[87] Vispoel B, Gamache RR. Modified Complex Robert-Bonamy calculations of line shape parameters for the CO_2-H_2O collision system. J Quant Spectrosc Radiat Transfer 2024;316:108896. http://dx.doi.org/10.1016/j.jqsrt.2024.108896.

[88] Iwakuni K, Okubo S, Yamada KMT, Inaba H, Onae A, Hong FL, et al. Ortho-para-dependent pressure effects observed in the near infrared band of acetylene by dual-comb spectroscopy. Phys Rev Lett 2016;117:143902. http://dx.doi.org/10.1103/PhysRevLett.117.143902.

[89] Hartmann JM, Tran H. Comment on ortho-para-dependent pressure effects observed in the near infrared band of acetylene by dual-comb spectroscopy. Phys Rev Lett 2017;119:069401. http://dx.doi.org/10.1103/PhysRevLett.119.069401.

[90] Newville M, Otten R, Nelson A, Stensitzki T, Ingargiola A, Allan D, et al. lmfit/lmfit-py: 1.2.1. Zenodo 2023. http://dx.doi.org/10.5281/zenodo.7887568.

[91] Ben-Reuven A, Kimel S, Hirshfeld MA, Jaffe JH. Theory and measurement of pressure-induced shifts of HCl lines due to noble gases. J Chem Phys 1961;35:955–62. http://dx.doi.org/10.1063/1.1701245.

[92] Petrova T, Solodov A, Solodov A, Deichuli V, Starikov V. Measurements and calculations of Ar-broadening parameters of water vapour transitions in a wide spectral region. Mol Phys 2017;115:1642–56. http://dx.doi.org/10.1080/00268976.2017.1311422.

[93] Werner HJ, Knowles PJ, Manby FR, Black JA, Doll K, Heßelmann A others. The Molpro quantum chemistry package. J Chem Phys 2020;152:144107. http://dx.doi.org/10.1063/5.0005081.

[94] Kobus J, Moncrieff D, Wilson S. Comparison of the polarizabilities and hyperpolarizabilities obtained from finite basis set and finite difference Hartree–Fock calculations for diatomic molecules. J Phys B: At Mol Opt Phys 2001;34:5127. http://dx.doi.org/10.1088/0953-4075/34/24/314.

[95] Chubb KL, Tennyson J, Yurchenko SN. ExoMol Molecular linelists – XXXVII: spectra of acetylene. Mon Not R Astron Soc 2020;493:1531–45. http://dx.doi.org/10.1093/mnras/staa229.

[96] Chubb KL, Joseph M, Franklin J, Choudhury N, Furtenbacher T, Császár AG, et al. MARVEL analysis of the measured high-resolution spectra of C_2H_2. J Quant Spectrosc Radiat Transfer 2018;204:42–55. http://dx.doi.org/10.1016/j.jqsrt.2017.08.018.

[97] Chubb KL, Yachmenev A, Tennyson J, Yurchenko SN. Treating linear molecule HCCH in calculations of rotation-vibration spectra. J Chem Phys 2018;149:014101. http://dx.doi.org/10.1063/1.5031844.

[98] Yurchenko SN, Amundsen DS, Tennyson J, Waldmann IP. A hybrid line list for CH_4 and hot methane continuum. Astron Astrophys 2017;605:A95. http://dx.doi.org/10.1051/0004-6361/201731026.

[99] Yurchenko SN, Yachmenev A, Ovsyannikov RI. Symmetry adapted ro-vibrational basis functions for variational nuclear motion: TROVE approach. J Chem Theory Comput 2017;13(9):4368–81. http://dx.doi.org/10.1021/acs.jctc.7b00506.

[100] D.M. Bishop. Molecular vibrational and rotational motion in static and dynamic electric fields. Rev Modern Phys 1990;62:343–74. http://dx.doi.org/10.1103/RevModPhys.62.343.

[101] Thibault F, Corretja B, Viel A, Bermejo D, Martínez RZ, Bussery-Honvault B. Linewidths of C_2H_2 perturbed by H_2: experiments and calculations from an ab initio potential. Phys Chem Chem Phys 2008;10:5419. http://dx.doi.org/10.1039/b804306j.

[102] Wilzewski JS, Gordon IE, Kochanov RV, Hill C, Rothman LS. H_2, He, and CO_2 line-broadening coefficients, pressure shifts and temperature-dependence exponents for the HITRAN database. Part 1: SO_2, NH_3, HF, HCl, OCS and C_2H_2. J Quant Spectrosc Radiat Transfer 2016;168:193–206. http://dx.doi.org/10.1016/j.jqsrt.2015.09.003.

[103] DePristo AE, Augustin SD, Ramaswamy R, Rabitz H. Quantum number and energy scaling for nonreactive collisions. J Chem Phys 1979;71:850–65. http://dx.doi.org/10.1063/1.438376.

[104] DePristo AE, Rabitz H. The effect of elastic and reorientation collisions on vibration–rotation lineshapes: A semi-empirical approach. J Quant Spectrosc Radiat Transfer 1979;22:65–79. http://dx.doi.org/10.1016/0022-4073(79)90107-9.

[105] Waldman M, Hagler A. New combining rules for rare gas van der waals parameters. J Comput Chem 1993;14:1077–84. http://dx.doi.org/10.1002/jcc.540140909.

[106] Moszynski R, Wormer PES, van der Avoird A. Ab initio potential energy surface and near-infrared spectrum of the He-C_2H_2 complex. J Chem Phys 1995;102:8385–97. http://dx.doi.org/10.1063/1.468830.

[107] Thibault F, Vieuxmaire O, Sizun T, Bussery-Honvault B. An ab initio potential energy surface for the C_2H_2–N_2 system. Mol Phys 2012;110:2761–71. http://dx.doi.org/10.1080/00268976.2012.718380.

[108] Karim F, Scholten SK, Perrella C, Luiten AN. Rapid generation of massive thermodynamic datasets using frequency comb spectroscopy. J Chem Phys 2024;160:104304. http://dx.doi.org/10.1063/5.0191103.

[109] Bukowski R, Sadlej J, Jeziorski B, Jankowski P, Szalewicz K, Kucharski SA, et al. Intermolecular potential of carbon dioxide dimer from symmetry-adapted perturbation theory. J Chem Phys 1999;110:3785–803. http://dx.doi.org/10.1063/1.479108.

[110] Hu R, Bello-Arufe M, Paragas K, Zilinskas M, van Buchem C others. A secondary atmosphere on the rocky Exoplanet 55 Cancri e. Nature 2024;1–2. http://dx.doi.org/10.1038/s41586-024-07432-x.

[111] kumar Pal A, kumar N, Kshirsagar RJ. Measurement of self-broadening coefficients and line intensities of $\nu_1+\nu_3+\nu_4$ - ν_4 band of acetylene in 1.5 μm spectral region: External cavity diode laser based absorption study. J Quant Spectrosc Radiat Transfer 2023;300:108510. http://dx.doi.org/10.1016/j.jqsrt.2023.108510.

[112] Ida T, Ando M, Toraya H. Extended pseudo-Voigt function for approximating the Voigt profile. J Appl Crystallogr 2000;33:1311–6. http://dx.doi.org/10.1107/S0021889800010219.

[113] Ma Q, Boulet C, Tipping RH. Vibrational dependence of line coupling and line mixing in self-broadened parallel bands of NH_3. J Quant Spectrosc Radiat Transfer 2017;203:425–33. http://dx.doi.org/10.1016/j.jqsrt.2017.01.010.

[114] Lamouroux J, Gamache RR, Laraia AL, Hartmann JM, Boulet C. Semiclassical calculations of half-widths and line shifts for transitions in the 30012←00001 and 30013←00001 bands of CO_2. III: Self collisions. J Quant Spectrosc Radiat Transfer 2012;113:1536–46. http://dx.doi.org/10.1016/j.jqsrt.2012.03.035.

[115] Hartmann JM, Boulet C. Line shape parameters for HF in a bath of argon as a test of classical path models. J Chem Phys 2000;113:9000–10. http://dx.doi.org/10.1063/1.1319346.

[116] Gamache RR, Vispoel B. On the temperature dependence of half-widths and line shifts for molecular transitions in the microwave and infrared regions. J Quant Spectrosc Radiat Transfer 2018;217:440–52. http://dx.doi.org/10.1016/j.jqsrt.2018.05.019.

[117] Wcislo P, Thibault F, Stolarczyk N, Jozwiak H, Slowinski M, Gancewski M, et al. The first comprehensive dataset of beyond-Voigt line-shape parameters from ab initio quantum scattering calculations for the HITRAN database: He-perturbed H_2 case study. J Quant Spectrosc Radiat Transfer 2021;260:107477. http://dx.doi.org/10.1016/j.jqsrt.2020.107477.

[118] Barton EJ, Hill C, Czurylo M, Li HY, Hyslop A, Yurchenko SN, et al. The ExoMol diet: H_2 and He line-broadening parameters. J Quant Spectrosc Radiat Transfer 2017;203:490–5. http://dx.doi.org/10.1016/j.jqsrt.2017.01.028.

[119] Antony BK, Neshyba S, Gamache RR. Self-broadening of water vapor transitions via the complex Robert–Bonamy theory. J Quant Spectrosc Radiat Transfer 2007;105:148–63. http://dx.doi.org/10.1016/j.jqsrt.2006.10.005.

[120] Luo Y, Ågren H, Vahtras O, Jørgensen P, Spirko V, Hettema H. Frequency-dependent polarizabilities and first hyperpolarizabilities of H_2O. J Chem Phys 1993;98:7159–64. http://dx.doi.org/10.1063/1.464733.

[121] Starikov VI, Petrova TM, Solodov AM, Solodov AA, Deichuli VM. Study of the H_2O dipole moment and polarisability vibrational dependence by the analysis of rovibrational line shifts. Spectra Chimica Acta A 2019;210:275–80. http://dx.doi.org/10.1016/j.saa.2018.11.032.

[122] Herman M, Campargue A, El Idrissi MI, Vander Auwera J. Vibrational spectroscopic database on acetylene, $\tilde{X}\ ^1\Sigma_g^+$ ($^{12}C_2H_2$, $^{12}C_2D_2$, and $^{13}C_2H_2$). J Phys Chem Ref Data 2003;32:921–1361. http://dx.doi.org/10.1063/1.1531651.